Electrostatically Embedded Multiconfiguration Molecular Mechanics Based on the Combined Density Functional and Molecular Mechanical Method

Masahiro Higashi and Donald G. Truhlar*

Department of Chemistry and Supercomputing Institute, 207 Pleasant Street SE,

University of Minnesota, Minneapolis, Minnesota 55455-0431

*truhlar@umn.edu

ABSTRACT: We present a new method for generating global or semi-global potential energy surfaces in the presence of an electrostatic potential; the new method can be used to model chemical reactions in solution or in an enzyme, nanocavity, or other chemical environment. The method extends the multiconfiguration molecular mechanics (MCMM) method so that the energy depends on the electrostatic potential at each atomic center. The charge distribution of the system can also be calculated. We illustrate the method by applying it to the symmetric bimolecular reaction $Cl^- + CH_3Cl' \rightarrow ClCH_3 + Cl'^-$ in aqueous solution, where the potential energy information is obtained by the combined density functional and molecular mechanical (DF/MM) method, that is by the combined quantum mechanical and molecular mechanical method (QM/MM) with the QM level being density functional theory. It is found that we can describe a semi-global potential energy surface in aqueous solution with electronic structure information obtained entirely in the gas phase, including the linear and quadratic responses to variations in the electrostatic potential distribution. The semi-global potential energy surface calculated by the present method is in good agreement with that calculated directly without any fitting.

1. Introduction

Combined quantum mechanical and molecular mechanical (QM/MM) methods have provided powerful means for studying chemical reactions in solution, enzymes, and solids.[1-28] In these approaches, the solute molecule or the reaction center involved in the formation and breaking of chemical bonds is described quantum mechanically, while the surroundings (e.g. solvent or protein environment) are treated by using a molecular mechanics (MM) force field. When the system contains a large number of atoms, a statistical sampling method such as molecular dynamics (MD) or Monte Carlo simulation is required.

However, the high computational cost of *ab initio* or density functional QM calculations prevents carrying out QM/MM MD simulations with reliable accuracy and adequate sampling. To overcome this difficulty, many more approximate methods have been developed, but we can mainly classify them into three types. In the first type of method, a reaction path connecting the reactant and product is first determined in limited dimensionality, e.g., in the gas phase or with non-quantal degrees of freedom (corresponding to spectator atoms or a secondary zone) excluded (in which case the method is called QM-FE) or frozen (in which case it is called QM/MM-FE). Then the free energy profile is obtained by free energy perturbation calculations along the path with the QM coordinates and electron density fixed.[29-36] These methods assume that the dynamics of the QM and MM subsystems are independent of each other and that the QM subsystem needs to be treated only in the quadratic region around the single uncoupled path.[37] Although several efficient algorithms for tracing the reaction paths have been developed,[30,33-35] this approach sometimes has a difficulty that the reaction path is trapped at one of the local minima of the potential energy surface (PES) and not smoothly connected from the reactant to product because there are many local minima on the MM PES.[32] Any single reaction path can deviate significantly from paths that make an appreciable contribution in a properly sampled thermal ensemble,[38-48] even if the single path is the minimum-free-energy path (MFEP) on the potential of mean force (PMF) for a large subset of the degrees of freedom. (The PMF is an averaged energy surface, in particular a free energy surface (FES). The true dynamics involves an average over paths, not the

optimized path on an average surface, and, even if the subset of the degrees of freedom included in the potential of mean force were large enough, this potential provides the full information needed to describe the dynamics only if classical transition state theory applies with a transmission coefficient of unity.) In addition, since the QM coordinates and charge distribution are fixed during MD simulations of this type, a significant part of the coupling between the QM and MM regions is ignored.

In the second type of calculation, high-level electronic structure methods combined with dielectric continuum models[49-54] or integral equation theories of solvation (such as the reference interaction site model self-consistent field (RISM-SCF) method[55-58]) are used to calculate the free energy surfaces of chemical reactions in solution. Although these methods do not need to sample the solvent degrees of freedom, they cannot easily be applied to reactions with inhomogeneous environments such as proteins, and furthermore they again yield only a pre-averaged surface. (For many purposes, it is an advantage to directly calculate the FES, and it facilitates the calculation of equilibrium solvation paths[59,60] (ESPs), also called minimum free-energy paths[61] (MFEPs), and transition state theory rate constants,[53] but the PES required for full real-time dynamics can only be obtained from the FES by making further approximations.[62,63] Note that an ESP is a special case of an MFEP in which the primary coordinates on which the FES depends correspond to the coordinates of a solute or a microsolvated solute and the secondary subsystem that is averaged corresponds to the solvent or the rest of the solvent.)

In the third type of calculation (SE-MO/MM), one uses proper free energy sampling of unaveraged motions, but due to cost, one uses semiempirical molecular orbital (SE-MO) methods such as Austin model 1 (AM1),[64] parametrized model 3 (PM3),[65] or self-consistent-charge density-functional tight binding (SCC-DFTB)[66,67] instead of high-level methods in the QM electronic structure calculation. Semiempirical methods require much lower computational cost than *ab initio* or density functional methods, and direct SE-MO/MM dynamics simulations are feasible, so dynamical properties such as transmission coefficients can be calculated straightforwardly.[16,47] However, it is well known that SE-MO is less reliable than *ab initio* wave function theory and density functional theory.

Lu and Yang[37] re-examined the QM/MM-FE method[30,34] and summarized its chief approximations as (i) assuming that the dynamics of the QM and MM subsystems are independent of each other and (ii) assuming that the QM system is confined to the quadratic region around the single uncoupled path. They then proposed a new method, called QM/MM-RPP where the PES and its electron density response properties are expanded to second order along a reaction path.[37] The expanded potential and response properties provide what may be called a reaction path potential (RPP), which is a concept widely used in gas-phase dynamics.[68-74] Yang and coworkers[61] subsequently extended the theory to optimize the reaction path on an FES; they call the resulting theory the QM/MM minimum free-energy path (QM/MM-MFEP) method. This method can treat the dynamical coupling between the QM and MM regions with QM/MM methods employing high-level QM in the vicinity of the MFEP. However, a second-order expansion is valid only near the origin of the expansion, and many expansion points are required to calculate a global FES. A global PES or global FES is needed to compute a broad distribution of reaction paths such as, for example, are often involved in large-curvature tunneling, which can make a significant contribution to the rate of hydrogen transfer reactions such as proton transfer reactions. For this purpose, and because even for the small-curvature tunneling case the ensemble of reaction paths can be broad,[47] it is desirable to develop a method to describe the global PES with a minimum of high-level QM input. This is the objective of the present study.

The multiconfiguration molecular mechanics (MCMM) method will be the starting point for the present development. MCMM has been successful in describing semi-global potential energy surfaces of gas-phase reactions and calculating the reaction rates with multidimensional tunneling contributions.[75-82] In the MCMM method, which is compared elsewhere[83,84] (with more than 30 references) to related approaches, the Born-Oppenheimer potential energy at geometry $\mathbf{q}$ is represented as the lowest eigenvalue of the 2×2 diabatic Hamiltonian matrix,

$$\mathbf{V}^{\text{MCMM}}(\mathbf{q}) = \begin{pmatrix} V_{11}(\mathbf{q}) & V_{12}(\mathbf{q}) \\ V_{12}(\mathbf{q}) & V_{22}(\mathbf{q}) \end{pmatrix}, \tag{1}$$

where the diagonal elements, V_{11} and V_{22}, are MM energy functions that describe reactants and products, respectively. The off-diagonal element V_{12} and its derivatives are determined to reproduce high-level electronic structure calculation of the energy, gradient, and Hessian at some reference points called Shepard points, and modified Shepard interpolation.[85,86] is used to interpolate the PES between the trust regions of the resulting set of second-order Taylor series. In case of reactions with more than one possible product, MCMM would need to be extended, e.g., to use a 3×3 matrix. The computational cost of using MCMM is much lower than that of using high-level electronic structure calculations directly.

In the present paper, we propose a method called electrostatically embedded multiconfiguration molecular mechanics (EE-MCMM). The new method is based on QM/MM methodology, and it extends the original MCMM by adding the electrostatic potential on each QM atom from the MM regions to $\mathbf{V}^{MCMM}$. Taylor expansions are carried out with respect to both the nuclear coordinates and the electrostatic potentials at the nuclei; the coefficients of the Taylor series are determined such that they reproduce high-level electronic structure calculations at Shepard points. The collection of the values of the external electrostatic potential at the locations of the QM nuclei will be called the electrostatic potential distribution. The EE-MCMM allows us to calculate the PES in the presence of an external electrostatic potential. The Taylor series can represent the electrostatic potential due to the MM subsystem, and thus EE-MCMM can describe semi-global PESs with moderate computational cost. Because the method is efficient, we can use DF/MM, that is, QM/MM with the QM level being density functional theory.

We illustrate the new method by application to the symmetric bimolecular reaction $Cl^- + CH_3Cl' \rightarrow ClCH_3 + Cl'^-$ in aqueous solution, a reaction that has been investigated with various theoretical methods.[29,87-108] We first create a semi-global PES in the gas phase by MCMM. The PES generated by MCMM is compared to that calculated directly without any fitting in a wide swath from the reactant through the saddle point to the product. We also calculate the variation of the gas-phase charge distribution (i.e., the partial charges on the QM atoms) along the reaction path in the gas phase

by EE-MCMM, and we evaluate the response of the gas-phase partial charges and energy to the electrostatic potential distribution through second order in the Taylor series. Then we apply the EE-MCMM method to the same reaction in solution, where we use the geometries and electrostatic potentials calculated by the RISM-SCF method[55-57] to compare full RISM-SCF calculations to results predicted by EE-MCMM calculations with all the electrostatic potentials at the Shepard points equal to zero. We employ the same Shepard points as in the gas phase. After the reliability of the EE-MCMM is checked in the case that only the electrostatic potential is changed, we compare the PES of EE-MCMM calculations to full high-level calculations along an aqueous-solution reaction path. Note that when we talk about the PES in a liquid-phase solution, we are referring to the electrostatically embedded electronic energy (including nuclear repulsion) of the QM subsystem. The variation of the charge distribution along the reaction path in the aqueous solution is also computed.

The organization of the article is as follows. In the next section, we describe the theoretical methods employed here. The computational details of the EE-MCMM calculations are given in section 3. In section 4, we present the results of the calculations, and the conclusions are summarized in section 5.

2. Theoretical method

In QM/MM methods, the potential energy is represented as the sum of three terms,

$$V^{\text{total}}(\mathbf{R}, \mathbf{R}^{\text{MM}}) = V^{\text{QM}}(\mathbf{R}, \mathbf{R}^{\text{MM}}) + V^{\text{QM/MM}}(\mathbf{R}, \mathbf{R}^{\text{MM}}) + V^{\text{MM}}(\mathbf{R}^{\text{MM}}), \tag{2}$$

where $\mathbf{R}$ and $\mathbf{R}^{\text{MM}}$ stand for the collection of the coordinates $\mathbf{R}_a$ and $\mathbf{R}_A^{\text{MM}}$ of atoms in the QM and MM regions, respectively, where $a = 1, 2, \ldots, n_1$ and $A = 1, 2, \ldots, n_2$. Here the first term is the electronic energy of the QM region, $V^{\text{QM}} = \langle \Psi | \hat{H}_0 | \Psi \rangle$, with Ψ being the electronic wave function and $\hat{H}_0$ the electronic Hamiltonian (including nuclear repulsions) of the QM region. Note that although $\hat{H}_0$ depends only on $\mathbf{R}$, Ψ depends on $\mathbf{R}^{\text{MM}}$ as well as $\mathbf{R}$ through $V^{\text{QM/MM}}$. The last term in Eq. (2) is the MM potential energy function. The QM/MM interaction term $V^{\text{QM/MM}}(\mathbf{R}, \mathbf{R}^{\text{MM}})$ can be separated into three terms,

$$V^{\text{QM/MM}}(\mathbf{R}, \mathbf{R}^{\text{MM}}) = V_{\text{ele}}^{\text{QM/MM}}(\mathbf{R}, \mathbf{R}^{\text{MM}}) + V_{\text{vdW}}^{\text{QM/MM}}(\mathbf{R}, \mathbf{R}^{\text{MM}}) + V_{\text{val}}^{\text{QM/MM}}(\mathbf{R}, \mathbf{R}^{\text{MM}}), \tag{3}$$

where $V_{\text{ele}}^{\text{QM/MM}}$, $V_{\text{vdW}}^{\text{QM/MM}}$ and $V_{\text{val}}^{\text{QM/MM}}$ are the electrostatic, van der Waals, and valence interaction energies, respectively. Of these three terms, only $V_{\text{ele}}^{\text{QM/MM}}$ depends on Ψ. We define the sum of the Ψ-dependent terms, V^{QM} and $V_{\text{ele}}^{\text{QM/MM}}$, as the electrostatically embedded QM energy:

$$V^{\text{EEQM}}(\mathbf{R}, \mathbf{R}^{\text{MM}}) \equiv V^{\text{QM}}(\mathbf{R}, \mathbf{R}^{\text{MM}}) + V_{\text{ele}}^{\text{QM/MM}}(\mathbf{R}, \mathbf{R}^{\text{MM}}). \tag{4}$$

The objective of the present study is to reproduce this $V^{\text{EEQM}}(\mathbf{R}, \mathbf{R}^{\text{MM}})$ by the EE-MCMM method. Note that V^{EEQM} is called the PES.

We adopt a site-site representation of the QM/MM electrostatic interaction,[55,108-112]

$$V_{\text{ele}}^{\text{QM/MM}}(\mathbf{R}, \mathbf{R}^{\text{MM}}) = \langle \Psi | \hat{\mathbf{Q}}^{\text{T}} \mathbf{\Phi} | \Psi \rangle, \tag{5}$$

where $\hat{Q}_a$ is the population operator that generates the partial charge Q_a on the QM atomic site a,

$$Q_a = \left\langle \Psi \middle| \hat{Q}_a \middle| \Psi \right\rangle, \tag{6}$$

and Φ_a is the electrostatic potential from the MM region,

$$\Phi_a = \sum_{A=1}^{n_2} \frac{Q_A^{MM}}{\left| \mathbf{R}_a - \mathbf{R}_A^{MM} \right|}, \tag{7}$$

where Q_A^{MM} is the effective charge of MM atom A. Note that $\mathbf{Q}$ and $\mathbf{\Phi}$ are n_1-dimensional vectors, and $\mathbf{R}_a$ and $\mathbf{R}_A^{MM}$ are 3-dimentional vectors. By adopting this representation, we can regard V^{EEQM} as a function of $\mathbf{R}$ and $\mathbf{\Phi}$,

$$V^{EEQM}\left(\mathbf{R}, \mathbf{\Phi} \right) = \left\langle \Psi \middle| \hat{H}_0 + \hat{\mathbf{Q}}^T \mathbf{\Phi} \middle| \Psi \right\rangle, \tag{8}$$

where $\mathbf{R}$ is a $3n_1$-dimensional vector. At this stage, we can extend the MCMM method[75] to the EE-MCMM one straightforwardly.

As in the MCMM method, the potential energy in EE-MCMM is the lowest eigenvalue of a 2×2 diabatic Hamiltonian matrix,

$$\mathbf{V}^{EE\text{-}MCMM}\left(\mathbf{q}, \mathbf{\Phi} \right) = \begin{pmatrix} V_{11}\left(\mathbf{q}, \mathbf{\Phi} \right) & V_{12}\left(\mathbf{q}, \mathbf{\Phi} \right) \\ V_{12}\left(\mathbf{q}, \mathbf{\Phi} \right) & V_{22}\left(\mathbf{q}, \mathbf{\Phi} \right) \end{pmatrix}, \tag{9}$$

where we use nonredundant or redundant internal coordinates[113] $\mathbf{q}$ to represent the nuclear coordinates of the QM subsystem. We evaluate $V^{EE\text{-}MCMM}$ and its derivatives in terms of the internal coordinates $\mathbf{q}$; then we transform the derivatives to the Cartesian coordinate system $\mathbf{R}$. The strategy to be developed involves evaluating a second-order Taylor expression of $V^{EE\text{-}MCMM}$ around a set of interpolation nodes $\left(\mathbf{R}^{(k)}, \mathbf{\Phi}^{(k)} \right)$, where $k = 1, 2, \ldots, N$, then converting[114] these expansions, for given V_{11} and V_{22}, to

second-order expansions of V_{12}^2 around the interpolation nodes (called Shepard points), and finally evaluating V_{12}^2 at any arbitrary geometry by Shepard interpolation[85,86] of these expressions.

The lowest eigenvalue of Eq. (9) is given by

$$V^{\text{EE-MCMM}}(\mathbf{q},\mathbf{\Phi}) = \frac{1}{2}\left\{ \left(V_{11}(\mathbf{q},\mathbf{\Phi})+V_{22}(\mathbf{q},\mathbf{\Phi})\right) - \left[\left(V_{11}(\mathbf{q},\mathbf{\Phi})-V_{22}(\mathbf{q},\mathbf{\Phi})\right)^2 - 4V_{12}(\mathbf{q},\mathbf{\Phi})^2\right]^{\frac{1}{2}}\right\}, \quad (10)$$

where $V_{11}(\mathbf{q},\mathbf{\Phi})$ and $V_{22}(\mathbf{q},\mathbf{\Phi})$ are analytic functions that describe V in the regions of reactants and products. $V_{12}(\mathbf{q},\mathbf{\Phi})$ is evaluated by Shepard interpolation[85,86] as follows:[75]

$$V_{12}(\mathbf{q},\mathbf{\Phi}) = \sum_{k=1}^{N} W_k(\mathbf{q},\mathbf{\Phi})V_{12}'(\mathbf{q},\mathbf{\Phi};k), \quad (11)$$

where $W_k(\mathbf{q},\mathbf{\Phi})$ is a normalized weight function,

$$\left[V_{12}'(\mathbf{q},\mathbf{\Phi};k)\right]^2 = \left[V_{12}(\mathbf{q},\mathbf{\Phi};k)\right]^2 u(\mathbf{q},\mathbf{\Phi};k) \quad (12)$$

where

$$u(\mathbf{q},\mathbf{\Phi};k) = \begin{cases} \exp\left(-\delta\big/\left[V_{12}(\mathbf{q},\mathbf{\Phi};k)\right]^2\right) & \left[V_{12}(\mathbf{q},\mathbf{\Phi};k)\right]^2 > 0 \\ 0 & \left[V_{12}(\mathbf{q},\mathbf{\Phi};k)\right]^2 \leq 0, \end{cases} \quad (13)$$

δ is a parameter (we used a very small value of δ, in particular $1\times10^{-8}\ E_{\text{h}}^2$ where $E_{\text{h}} \equiv 1$ hartree), and

$$\left[V_{12}(\mathbf{q},\mathbf{\Phi};k)\right]^2 = D^{(k)}\left[1 + \begin{pmatrix}\mathbf{b}_{\mathbf{q}}^{(k)\text{T}} & \mathbf{b}_{\mathbf{\Phi}}^{(k)\text{T}}\end{pmatrix}\begin{pmatrix}\Delta\mathbf{q}^{(k)} \\ \Delta\mathbf{\Phi}^{(k)}\end{pmatrix} + \frac{1}{2}\begin{pmatrix}\Delta\mathbf{q}^{(k)\text{T}} & \Delta\mathbf{\Phi}^{(k)\text{T}}\end{pmatrix}\begin{pmatrix}\mathbf{c}_{\mathbf{qq}}^{(k)} & \mathbf{c}_{\mathbf{q\Phi}}^{(k)} \\ \mathbf{c}_{\mathbf{\Phi q}}^{(k)} & \mathbf{c}_{\mathbf{\Phi\Phi}}^{(k)}\end{pmatrix}\begin{pmatrix}\Delta\mathbf{q}^{(k)} \\ \Delta\mathbf{\Phi}^{(k)}\end{pmatrix}\right], \quad (14)$$

$$\Delta\mathbf{q}^{(k)} = \mathbf{q} - \mathbf{q}^{(k)}, \quad (15)$$

and

$$\Delta\mathbf{\Phi}^{(k)} = \mathbf{\Phi} - \mathbf{\Phi}^{(k)}. \quad (16)$$

9

For $k = 1, 2, \ldots, N$, the Taylor series coefficients, $D^{(k)}$, $\mathbf{b}_{\mathbf{q}}^{(k)}$, $\mathbf{b}_{\mathbf{\Phi}}^{(k)}$, $\mathbf{c}_{\mathbf{qq}}^{(k)}$, $\mathbf{c}_{\mathbf{q\Phi}}^{(k)}$, $\mathbf{c}_{\mathbf{\Phi q}}^{(k)}$ and $\mathbf{c}_{\mathbf{\Phi\Phi}}^{(k)}$ are determined to reproduce V^{EEQM} in Eq. (8) and its first and second derivatives with respect to $\mathbf{q}$ and $\mathbf{\Phi}$ at the Shepard point $\left(\mathbf{q}^{(k)} \quad \mathbf{\Phi}^{(k)} \right)$. The expressions for the elements $D^{(k)}$, $\mathbf{b}_{\mathbf{q}}^{(k)}$, and $\mathbf{c}_{\mathbf{qq}}^{(k)}$ are given in Refs. 75 and 82. The other elements are obtained similarly. It is notable that EE-MCMM is the same as the original MCMM in the case when $\mathbf{\Phi} = \mathbf{0}$ and all $\mathbf{\Phi}^{(k)}$ (for $k = 1, 2, \ldots, N$) are also $\mathbf{0}$.

To implement the above procedure, we need the derivatives of electronic structure calculations of $V^{\mathrm{EEQM}}(\mathbf{R}, \mathbf{\Phi})$ with respect to $\mathbf{\Phi}$ in addition to those with respect to $\mathbf{R}$. The first derivative of $V^{\mathrm{EEQM}}(\mathbf{R}, \mathbf{\Phi})$ with respect to a component of $\mathbf{\Phi}$ is given by[110]

$$\frac{\partial V^{\mathrm{EEQM}}}{\partial \Phi_a} = \left\langle \Psi \left| \hat{Q}_a \right| \Psi \right\rangle = Q_a. \tag{17}$$

Then the second partial derivatives of $V(\mathbf{q}, \mathbf{\Phi})$ are

$$\frac{\partial^2 V^{\mathrm{EEQM}}}{\partial \Phi_a \partial \Phi_b} = \frac{\partial Q_a}{\partial \Phi_b} \equiv \chi_{ab}, \tag{18}$$

and

$$\frac{\partial^2 V^{\mathrm{EEQM}}}{\partial \Phi_a \partial R_b} = \frac{\partial Q_a}{\partial R_b} \equiv \kappa_{ab}. \tag{19}$$

These variables, χ_{ab} and κ_{ab}, are known as charge response kernels (CRKs); they describe the QM charge fluctuations due to the external electrostatic potential (which, in applications, will represent the electrostatic effect of the MM region) and to the displacements of the QM atoms. The CRKs χ_{ab} and κ_{ab} were introduced by Morita and Kato[110,111] and Lu and Yang[37] respectively. Since these effects are usually not included in MM potential energy functions, we define

$$V_{ii}(\mathbf{q}, \mathbf{\Phi}) = V_{ii}^{\mathrm{MM}}(\mathbf{q}) + V_{ii}^{\mathrm{CRK}}(\mathbf{q}, \mathbf{\Phi}), \tag{20}$$

where $V_{ii}^{\text{MM}}(\mathbf{q})$ is the MM potential energy function, and

$$V_{ii}^{\text{CRK}}(\mathbf{q},\mathbf{\Phi}) = \mathbf{Q}^{(i)\text{T}}\Delta\mathbf{\Phi}^{(i)} + \frac{1}{2}\Delta\mathbf{\Phi}^{(i)\text{T}}\mathbf{\kappa}^{(i)}\Delta\mathbf{\Phi}^{(i)} + \Delta\mathbf{\Phi}^{(i)\text{T}}\mathbf{\chi}^{(i)}\Delta\mathbf{q}^{(i)},\qquad(21)$$

where $\mathbf{Q}^{(i)}$, $\mathbf{\kappa}^{(i)}$, and $\mathbf{\chi}^{(i)}$ are calculated values at reactant and product, such that the partial charges and CRKs of EE-MCMM agree with electronic structure calculation at reactant and product, respectively. (Note that the reactant and product correspond to infinitely separated reagents and are not included in the N Shepard points used in Eq. (11), although we do include the precursor ion-dipole complex and the successor ion-dipole complex.) Then we can calculate the EE-MCMM potential energy and its derivatives. The calculation steps are the same as those in Refs. 75 and 82 except that $\mathbf{\Phi}$ is added.

3. Computational details

We used the MPW1K density functional[115] for the electronic structure calculations on the QM subsystem. The basis set is 6-31G(d,p) for C and H atoms and 6-31+G(d,p) for Cl. We refer to this mixed basis set as 6-31(+)G(d,p). Calculations carried out by direct dynamics, i.e., without MCMM or EE-MCMM, will be called direct or full.

Although there can be many choices for the population operator $\hat{Q}_a$, we choose the operator according to Charge Model 4 (CM4).[116] The CM4 charge model is determined from wave-function-dependent charges, the Mayer bond order,[117-119] and empirical parameters that are determined to reproduce experimental or converged theoretical charge-dependent observables,

$$Q_a = Q_a^0 + \sum_{b \neq a} B_{ab} \left(D_{ab} + C_{ab} B_{ab} \right), \tag{22}$$

where Q_a^0 is the partial atomic charge from either a Löwdin population analysis (LPA) for nondiffuse basis sets or a redistributed Löwdin population analysis (RLPA) for diffuse basis sets,[120] B_{ab} is the Mayer bond order between atom a and b, and D_{ab} and C_{ab} are empirical parameters. The RLPA charge is given by

$$Q_a^0 \left(\text{RLPA} \right) = Q_a^0 \left(\text{LPA} \right) + Z_a Y_a \sum_{b \neq a} \exp\left(-\alpha_a R_{ab}^2 \right) - \sum_{b \neq a} Z_b Y_b \exp\left(-\alpha_b R_{ab}^2 \right), \tag{23}$$

where Z_a is a empirical parameter, Y_a is the Löwdin population that is associated with the diffuse basis functions on atom a, and α_a is the diffuse orbital exponent on atom a. The Fock matrix and gradient for the Hamiltonian in Eq. (8) with CM4 charges are given in Refs. 121 and 122, respectively.

Although the CM4 parameters are available for various density functionals and basis sets, those for the MPW1K/6-31(+)G(d,p) mixed basis set are unavailable. The reason why we adopted the mixed basis set is that the wave function with MPW1K/6-31G+(d,p) in Eq. (8) was not converged for $\mathbf{\Phi} \neq \mathbf{0}$ at some geometries. Note that the fixed gas-phase density matrix at a geometry optimized in the gas phase could be used for B_{ab} in the previous study,[122] while this procedure is not appropriate for the present

study because the purpose of this study is to describe the global PES. We therefore determined the empirical parameters, D_{ab}, C_{ab}, and Z_a for MPW1K/6-31(+)G(d,p) so as to reproduce the CM4 charges obtained with MPW1K/6-31+G(d,p) in the gas phase at three geometries; CH_3Cl, the ion-molecule complex $Cl^-\cdots CH_3Cl$, and the saddle point $[Cl\cdots CH_3\cdots Cl]^-$. The optimized parameters are $D_{ab} = -0.02$ for a C and H pair, $D_{ab} = 0.11$ for a C and Cl pair, and $Z_a = 0.11$ for a Cl atom; the other parameters are set to zero. The mean unsigned error (MUE) and root-mean-square error (RMSE) of the CM4 charges between MPW1K/6-31+G(d,p) and MPW1K/6-31(+)G(d,p) at the three geometries are 3.6×10^{-3} and 4.9×10^{-3}, respectively. We obtained the Hessian and CRKs by numerical differentiations of the gradients and charges, respectively.

The gas-phase minimum energy path (MEP) was calculated by MCMM by the MC-TINKERATE program.[123] In these calculations, the MEP is the path of steepest descent in mass-scaled coordinates[124] from the saddle point, and the reaction coordinate is the signed distance along the path.

We employed the RISM-SCF method[55-57] to obtain the geometry and electrostatic potential $\mathbf{\Phi}$ on each atom from the MM region in aqueous solution. The reason why we adopted the RISM-SCF method in the present study is that we wanted to check, as a first step, how well the EE-MCMM method can reproduce V^{EEQM} at various geometries and with various electrostatic potential distributions. In the RISM-SCF method, the equilibrium distribution of MM solvent molecules can be calculated in a self-consistent manner. For a fixed subsystem consisting of the solute with coordinates $\mathbf{R}$ and averaging over a subsystem corresponding to the solvent, the FES is approximated as the sum of V^{QM} and the excess chemical potential $\Delta\mu$ coming from solute-solvent interaction:[57]

$$F(\mathbf{R}) = V^{QM}(\mathbf{R}) + \Delta\mu(\mathbf{R},\mathbf{Q}), \tag{24}$$

where $\Delta\mu$ is the standard-state free energy of solvation of a solute with fixed geometry $\mathbf{R}$[59]. Note that the FES is another name for a multidimensional potential of mean force.[125,126] This same quantity is also sometimes called[127] the solvent-modified potential energy of the system described by the coordinates $\mathbf{R}$.

In the RISM integral equation theory, in conjunction with the hyper-netted chain (HNC) closure relation,[128] $\Delta\mu$ can be expressed as[129]

$$\Delta\mu = -\frac{\rho}{\beta}\sum_a^{n_1}\sum_m^{N_v}\int_0^\infty\left[c_{am}(r_{am}) - \frac{1}{2}h_{am}^2(r_{am}) + \frac{1}{2}c_{am}(r_{am})h_{am}(r_{am})\right]4\pi r_{am}^2 dr_{am}, \qquad (25)$$

where r_{am} is the distance between an atom a of the QM solute molecule and an atom m of the MM solvent molecule, $r_{am} = |\mathbf{R}_a - \mathbf{R}_m^{MM}|$, N_v is the number of atoms contained in a solvent molecule ($N_v = 3$ for water), ρ is the density of solvent, $\beta = k_B T$ with k_B being the Boltzmann constant and T the temperature, and c_{am} and h_{am} are the direct and total correlation function, respectively. Note that c_{am} and h_{am} can be determined from the solute-solvent RISM equation and the HNC closure relation,

$$\tilde{h}_{am}(k_{am}) = \rho^{-1}\sum_b^{N_1}\sum_n^{N_v}\tilde{w}_{ab}(k_{ab})\tilde{c}_{bn}(k_{bn})\tilde{H}_{nm}(k_{nm}), \qquad (26)$$

and

$$h_{am}(r_{am}) = \exp\left[-\beta u_{am}(r_{am}) + h_{am}(r_{am}) - c_{am}(r_{am})\right] - 1, \qquad (27)$$

where w_{ab} is the intramolecular correlation function calculated using the QM solute coordinates $\mathbf{R}$, and H_{nm} is the pure solvent site density pair correlation function calculated from the solvent-solvent RISM equation; u_{am} is the solute-solvent interaction potential,

$$u_{am}(r_{am}) = \frac{Q_a Q_m^{MM}}{r_{am}} + 4\varepsilon_{am}\left\{\left(\frac{\sigma_{am}}{r_{am}}\right)^{12} - \left(\frac{\sigma_{am}}{r_{am}}\right)^6\right\}, \qquad (28)$$

where ε_{am} and σ_{am} is the Lennard-Jones parameters, and a tilde represents a Fourier transform with wavenumber k_{am} as in

$$\tilde{h}_{am}\left(k_{am}\right) = \frac{4\pi}{k_{am}} \int_0^\infty h_{am}\left(r_{am}\right) r_{am} \sin\left(k_{am} r_{am}\right) dr_{am} . \tag{29}$$

With this formalism, V^{QM} and $\mathbf{Q}$ in Eq. (24) can be determined by Eq. (8) with

$$\Phi_a = \rho \sum_m^{N_v} \int_0^\infty \frac{Q_m^{MM}}{r_{am}} g_{am}\left(r_{am}\right) 4\pi r_{am}^2 dr_{am} , \tag{30}$$

where g_{am} is the radial distribution function, and

$$g_{am} \equiv h_{am} - 1. \tag{31}$$

We can obtain the self-consistent free energy by iteratively solving Eqs. (8), (26), and (27) until self-consistency is achieved. The gradient of the free energy F can be calculated analytically.[57]

We optimized the QM geometry on the FES with one or two internal coordinates fixed, and then compared V^{EEQM} from the direct calculation (Eq. (8)) to $V^{EE\text{-}MCMM}$ from the EE-MCMM one (Eq. (10)) at the optimized coordinates and electrostatic potentials. We also calculated the minimum energy path[124] on the FES, and we refer to this as the MFEP. (Since the fixed system in our PMF is a solute, and the averaged subsystem is the solvent, we could also call this an ESP, but we use the more general term the rest of this article.)

In the RISM-SCF calculation, the Lennard-Jones parameters for the solute atoms were taken from the AMBER force field.[130] The simple point charge (SPC) model[131] was adopted for solvent water. The temperature and density of solvent water were 300 K and 1.0 g/cm^3, respectively. All the electronic structure calculations were performed by GAMESSPLUS[132] based on the GAMESS quantum package,[133] in which we implemented the RISM-SCF routines.

In the MCMM and EE-MCMM calculations, we used a modified MM3 force field[134-136] for the diagonal elements $V_{ii}^{MM}\left(\mathbf{q}\right)$ in Eq. (20). For the bond stretching term, we replaced the MM3 bond stretching function with a Morse[137] potential. The dissociation energy of the Morse function for C-Cl was set equal to 83.7 kcal/mol, which was calculated by MPW1K/6-31(+)G(d,p) and is in good

agreement with the experimental value, 83.8 kcal/mol.[138] We also modified the van der Waals energy term as in Ref. 81; we used the additional parameter $D = 0.01$ in the modified van der Waals energy function. The other parameters are the same as those installed in the TINKER program.[139] We used the same functional form for the normalized weight function as in the original MCMM method,[75]

$$W_k(\mathbf{q}) = \frac{\left(\dfrac{1}{d_k(\mathbf{q})}\right)^4}{\sum_{i=1}^{N}\left(\dfrac{1}{d_i(\mathbf{q})}\right)^4} , \tag{32}$$

where $d_k(\mathbf{q})$ denotes a generalized distance between $\mathbf{q}$ and $\mathbf{q}^{(k)}$, which is defined as

$$d_k(\mathbf{q}) = \sqrt{\sum_{j=1}^{j_{max}}\left(q_j - q_j^{(k)}\right)^2} . \tag{33}$$

We employed three bond distances ($j_{max} = 3$), C-Cl, C-Cl′, and Cl-Cl′, to calculate the generalized distance. We didn't make the weight function depend on $\mathbf{\Phi}$, although this is possible in principle. All the EE-MCMM calculations were carried out by the MC-TINKER program,[140] modified for this purpose.

4. Results and discussion

We applied the new EE-MCMM method to the reaction $Cl^- + CH_3Cl' \rightarrow ClCH_3 + Cl'^-$ in aqueous solution. The free energy profile of this reaction is much different in aqueous solution from that in the gas phase because the solute-solvent electrostatic interaction at the TS, where there is no dipole moment and the charge is more delocalized, is weaker than that at the reactant. Therefore, this reaction is a good benchmark system for testing the performance of theoretical methods, and consequently various methods have been applied to calculate the free energy profile of this reaction. [29,87-108]

For plotting purposes, we take the difference between two C-Cl distances as the reaction coordinate,

$$z = R_{CCl'} - R_{CCl} \tag{34}$$

although the reaction paths along which z and other quantities are computed are the gas-phase MEP and the aqueous-phase MFEP. First, in Fig. 1, we compare the gas-phase PES and the aqueous-phase FES with the former evaluated along the direct dynamics MEP and the latter along the direct MFEP. For each curve the zero of energy corresponds to infinitely separated reagents.

In the gas phase, the ion-dipole complex is 9.7 kcal/mol below reactants, and the potential energy barrier is 3.2 kcal/mol above reactants; both values are in good agreement with experimental values, 10.4[141] and 2.5[142] kcal/mol, respectively. (The best estimate of the gas-phase potential energy barrier is 3.1 kcal/mol.[143]) The ion-dipole complexes are found in the present calculations to be located at $z = \pm 1.378\,\text{Å}$.

In aqueous solution, the free energy barrier is calculated to be 25.8 kcal/mol, which agrees well with the experimental activation energy, 26.6 kcal/mol.[144] In contrast to the gas-phase reaction, the binding energy for the ion-dipole complex is calculated to be very small. A very shallow minimum (only -0.03 kcal/mol) was found in the FES at $z = 1.744\,\text{Å}$. Therefore, a practical objective for the EE-MCMM method is to reproduce the potential energy profile for $|z| \leq 1.8\,\text{Å}$.

4.1. Gas phase reaction

We first constructed a semi-global potential energy surface in gas phase by the original MCMM method. The objective region over which we aimed to make this valid was from the reactant ion-dipole complex through the saddle point (SP) to the product ion-dipole complex including the concave side of the reaction path. Note that the previous[75-82] MCMM studies did not attempt to converge the energy surface more than 3/4 of the way down from the barrier, but here we consider the path all the way down to the ion-dipole complexes. The placement of Shepard points was based on the strategy in Ref. 76, but some modifications were made, as described next.

The first MEP calculation was based on the MCMM-0 surface, which was constructed by electronic structure information at three geometries: the precursor ion-dipole complex, the SP, and the successor ion-dipole complex. (In general the notation[75,76] MCMM-N' means that the Shepard interpolation is based on Hessians at these three stationary points plus N' nonstationary points.) In the previous studies, we assumed that the V_{11} and V_{22} MM force fields could describe the PES of the local minima in the reactant and product valleys. Therefore, V_{12} was zero for these two points, which will here be called $k = N-1$ and $k = N$, where $N = N'+3$. In the present study, we used electronic structure calculations to determine a Taylor series of $V_{12}{}^2$ for all N points.

In order to keep the symmetry of the reaction, the nonstationary Shepard points were determined at the same time for both the reactant and product sides. We define the energy difference between the ion-dipole complex and the SP as V^*; this is 12.9 kcal/mol for MPW1K/6-31(+)G(d,p) in the gas phase. The first and second supplementary points ($\alpha = 1, 2$) were taken to be along the MEP of the MCMM-0 run, lower than the SP by 1/4 of V^*. The calculation with these five Shepard points is called MCMM-2 because it involves 2 supplementary points. The third and fourth supplementary points were taken to be along the MEP of the MCMM-2 run, lower than the SP by 1/2 of V^*. The calculation with these seven Shepard points is called MCMM-4. The fifth and sixth supplementary points were taken to be along the MEP of the MCMM-4 run, lower than the SP by 3/4 of V^*. This calculation is called MCMM-6. The

seventh and eighth supplementary points were taken to be along the MEP of the MCMM-6 run, lower than the SP by 7/8 of V^*. This calculation is called MCMM-8. We could connect from the SP to the reactant and product ion-dipole complex smoothly by the MCMM-8 MEP. To reproduce the PES on the concave side of the reaction path, a ninth supplementary point was taken to be located halfway in Cartesian coordinates along a line that connects the reactant ion-dipole complex with the product ion-dipole complex. The calculation including this point is called MCMM-9.

Therefore, we used the electronic structure information at 12 Shepard points (if we consider the symmetry, the number is reduced to 7). The locations of the Shepard points and the direct MEP are shown in Fig. 2. It is noted that the purpose of this study is not to reduce the number of Shepard points but to reproduce the semi-global PES in aqueous solution by EE-MCMM. It is possible to reduce the number of Shepard points by adjusting the force field parameters[81] or changing the strategy for where the Shepard points are placed.

The potential energy profiles of the direct, MCMM-0, MCMM-4 and MCMM-8 gas-phase calculations are shown in Fig. 3. The ends of the curves correspond to the precursor and successor ion-dipole complexes. The potential energies of the MCMM-0 and MCMM-4 calculations noticeably differ from the direct one, while the MCMM-8 potential curve is in good agreement with the direct one from the SP all the way to the ion-dipole complexes.

We present equipotential contour plots of the gas-phase PES determined in the MCMM-9 calculation in Fig. 4a. The length of the forming C-Cl bond and the breaking C-Cl′ bond are taken as the axes. The remaining coordinates are optimized by direct calculations. Equipotential contour plots of the difference between the MCMM-9 and direct PESs, $V^{MCMM} - V^{QM}$, are shown in Fig. 4b. In a wide swath from the precursor complex through the SP to the successor complex, including the concave side of the reaction path, the MCMM-9 PES agrees with the direct one within 1 kcal/mol. Therefore, this MCMM-9 PES is accurate enough for dynamics calculations.

The matrix elements of the electronically diabatic Hamiltonian $\mathbf{V}^{\text{MCMM}}$ and the lowest eigenvalue V^{MCMM} are plotted in Fig. 5 along four distinguished paths: the path with $R_{\text{CCl}} + R_{\text{CCl}'} = 4.6$ Å (Fig. 5a) which goes through the SP, the path with $R_{\text{CCl}} + R_{\text{CCl}'} = 5.0$ Å (Fig. 5b) which goes through the reactant and product ion-dipole complexes, the path with $R_{\text{CCl}} = 1.8$ Å which goes through the reactant ion-dipole complex (Fig. 5c), and the path with $R_{\text{CCl}} = 2.3$ Å which goes through the SP (Fig. 5d). The remaining coordinates are optimized by direct calculations. The matrix element V_{12} has a maximum at the SP, then decreases toward the reactant and product ion-dipole complexes.

To investigate the variation of the partial atomic charges along the reaction path, we carried out an EE-MCMM-9 calculation using the electronic structure information at the same Shepard points as MCMM-9. This means that all $\mathbf{\Phi}_a^{(k)}$ are zero for this EE-MCMM calculation. The partial charges can be obtained by calculating the derivative of $V^{\text{EE-MCMM}}$ in Eq. (10) with respect to $\mathbf{\Phi}$ as in Eq. (17), which yields

$$
Q_a = \frac{\partial V^{\text{EE-MCMM}}}{\partial \Phi_a} = \frac{1}{2} \left\{ \frac{\partial V_{11}}{\partial \Phi_a} + \frac{\partial V_{22}}{\partial \Phi_a} - \left[\frac{4V_{12}\dfrac{\partial V_{12}}{\partial \Phi_a} + \left[V_{11} - V_{22}\right]\left[\dfrac{\partial V_{11}}{\partial \Phi_a} - \dfrac{\partial V_{22}}{\partial \Phi_a}\right]}{\left[\left(V_{11} - V_{22}\right)^2 + 4V_{12}{}^2\right]^{1/2}} \right] \right\}. \tag{35}
$$

Note that the gas-phase charges correspond to evaluating this derivative with all $\mathbf{\Phi}_a = \mathbf{0}$. The partial charges on each atom in the EE-MCMM-9 and direct calculations along each MEP are presented in Fig. 6. By construction, the partial charges obtained by Eqs. (17) and (35) agree exactly at Shepard points, but the figure shows the changes of the partial charges in the MCMM-9 calculation are quite similar to those in the direct calculation along the whole reaction path. In both cases, the charges of two Cl atoms change significantly along the MEP.

4.2. Reaction in aqueous solution

Now we consider the PES for the reaction in aqueous solution; in particular we will compare $V^{\text{EE-MCMM}}$ to the electrostatically embedded QM energy V^{EEQM}.

When we apply the EE-MCMM method to a reaction in the condensed phase, where $\mathbf{\Phi} \neq \mathbf{0}$, we have to consider how the locations of the Shepard points $\left(\mathbf{q}^{(k)}, \mathbf{\Phi}^{(k)} \right)$ are determined. In general, it is desirable to select the Shepard points so as to make $\Delta\mathbf{q}^{(k)}$ and $\Delta\mathbf{\Phi}^{(k)}$ as small as possible during the statistical sampling in the simulation of the target QM/MM system because EE-MCMM is based on second- order expansions. Several strategies can be considered. One of the strategies, in analogy to the QM/MM-MFEP procedure of Yang and coworkers,[61] is to take the Shepard points along the QM/MM MFEP determined from the potential of mean force in the QM degrees of freedom. In this scheme, the QM geometry and charge distribution are fixed during an MD simulation, then the QM geometry is optimized using the average electrostatic potential and force from the MM atoms; this procedure is repeated until self-consistency between the QM and MM regions is achieved. If the ensemble of reaction paths were restricted to paths that lie close to the MFEP, then this kind of MFEP procedure would make $\Delta\mathbf{q}^{(k)}$ and $\Delta\mathbf{\Phi}^{(k)}$ always be small. A drawback to this scheme is that the computational cost of the MFEP calculation is not low. If we were to take supplementary Shepard points along the MFEP of a previous EE-MCMM calculation with fewer Shepard points (as was done in the original MCMM method), hundreds of MD simulation runs would be required, which is undesirable. Furthermore, one expects significant contributions to the reaction rates from paths that differ appreciably from the MFEP.[38-48]

Therefore, we adopted a different strategy for the location of the Shepard points in condensed-phase reactions. We first select Shepard points for a gas-phase reaction in the same way as in the original MCMM method, and then these Shepard points are applied to the reaction in aqueous solution. In other words, all the Shepard points have $\mathbf{\Phi}^{(k)} = \mathbf{0}$. This means that as far as the terms relating to the electrostatic potential distribution are concerned, the Taylor series is reduced to a Maclaurin series, or −

stated another way – we are using only gas-phase information as input to the Shepard interpolation for the aqueous-phase calculations. We adopted this simple strategy because it has been shown[111] that the linear response relation between $\mathbf{Q}$ and $\boldsymbol{\Phi}$ (see below), that is, a second order expansion of V^{EEQM} with respect to $\boldsymbol{\Phi}$, generally holds well even if the components of $\Delta\boldsymbol{\Phi}$ become quite large. Based on this result, we first generated a semi-global PES in the gas phase, and then we applied it to the reaction in aqueous solution. It is noted that the computational cost of this strategy is much lower than using a MFEP calculation since only QM gas-phase calculations on the solute are required during the stage of finding the reaction path. Although the present reaction was treated using only eight supplementary points near the gas-phase reaction path and one point off the path, other reactions may require more points off the reaction path. On the other hand one might be able to use fewer points near the reaction path if their locations are optimized. Further experience will be helpful in understanding these issues.

We first considered the case of $\Delta\mathbf{q} = \mathbf{0}$ and $\Delta\boldsymbol{\Phi} \neq \mathbf{0}$ to check the reliability. We used the RISM-SCF method to calculate the electrostatic potential on each atom of the solute in aqueous solution at the gas-phase precursor ion-dipole complex and the gas-phase SP. The calculated electrostatic potential distribution is given in Table 1. The electrostatic potential on the Cl ion is larger than those on other atoms at the gas-phase ion-dipole complex because Cl^- has a considerable localized negative charge. In contrast the electrostatic potential distribution is more uniform at the SP because the charge is more delocalized. We then compared the electrostatically embedded energies and charges of EE-MCMM (calculated with the $\boldsymbol{\Phi}$ of Table 1) to those of a direct calculation. We also compared the results with those calculated by the original CRK method,[110,111]

$$\mathbf{Q}\left(\text{CRK}\right) = \mathbf{Q}_0 + \boldsymbol{\chi}\,\boldsymbol{\Phi} \tag{36}$$

$$V^{\text{EEQM}}\left(\text{CRK}\right) = V_0^{\text{QM}} + \mathbf{Q}_0{}^{\text{T}}\boldsymbol{\Phi} + \frac{1}{2}\boldsymbol{\Phi}^{\text{T}}\boldsymbol{\chi}\,\boldsymbol{\Phi}\,, \tag{37}$$

where $\mathbf{Q}_0$ are the charges at $\mathbf{\Phi} = 0$, and V_0^{QM} is the value of $\langle \Psi_0 | \hat{H}_0 | \Psi_0 \rangle$, where Ψ_0 is the gas-phase wave function. The difference between $\langle \Psi | \hat{H}_0 | \Psi \rangle$ and $\langle \Psi_0 | \hat{H}_0 | \Psi_0 \rangle$ is accounted for by using the coefficient of 1/2 in the last term of Eq. (37). Note that the original CRK method and our method differ in the way that the expansion is carried out. The original CRK expands V^{EEQM} itself, while our method expands V_{12}^2 by using Eq. (14). The results are shown in Table 2. The aqueous charge distributions obtained by all the methods in Table 2 are more polarized than the gas-phase charge distribution because of the strong solute-solvent interaction. Both the degrees of charge polarization and the electrostatically embedded energy change upon solution are quite similar in all three methods; the differences are 0.1 kcal/mol or less.

We next calculated the profile of $V^{EE\text{-}MCMM}$ by EE-MCMM-9 along the direct MFEP that was obtained by the RISM-SCF method. The result is presented in Fig. 7. The energy is relative to separated reactants in the gas phase. Both edges of the potential energy profiles correspond to the shallow minima of the free energy profile obtained by RISM-SCF method. The energy difference between the SP and ion-dipole complex is very large compared with gas-phase reaction because of the difference of the solute-solvent interaction. The figure shows that the potential energy profile of EE-MCMM-9 is in very good agreement with that of the direct calculation; in fact the two curves are essentially on top of one another. We computed equipotential contour plots of $V^{EE\text{-}MCMM}$ as determined in the EE-MCMM-9 calculation; these are shown in Fig. 8a. The forming C-Cl bond and the breaking C-Cl′ bond are taken as the axes. The remaining coordinates and the electrostatic potential distribution are optimized by RISM-SCF calculations. Although $V^{EE\text{-}MCMM}$ has a minimum in Fig. 8a when both C-Cl distances are increased, neither V^{total} nor F has a minimum in this region. Equipotential contour plots of the difference between the EE-MCMM-9 and direct PESs, $V^{EE\text{-}MCMM} - V^{EEQM}$, are shown in Fig. 8b. As in the case of the gas-phase reaction, the EE-MCMM-9 PES agrees with the direct one within 1 kcal/mol in a wide swath from the reactant through the SP to the product including the concave side of the

reaction path. It is notable that we only used electronic structure information of the gas-phase reaction. Nevertheless, we could reproduce the PES for the condensed-phase reaction.

To investigate the effects of the electrostatic potential $\mathbf{\Phi}$ on the matrix elements of the electronically diabatic Hamiltonian $\mathbf{V}^{\text{EE-MCMM}}$, we computed these matrix elements along the distinguished path with $R_{\text{CCl}} + R_{\text{CCl}'} = 4.8$ Å for the following four sets of the electronic potential distributions: $\mathbf{\Phi} = \mathbf{0}$ (gas phase), $\mathbf{\Phi} = \mathbf{\Phi}^{\text{IDC}}$, $\mathbf{\Phi} = \mathbf{\Phi}^{\text{SP}}$, and $\mathbf{\Phi} = \frac{1}{2}\mathbf{\Phi}^{\text{SP}}$, where $\mathbf{\Phi}^{\text{IDC}}$ and $\mathbf{\Phi}^{\text{SP}}$ are the electrostatic potential distribution calculated by RISM-SCF at the gas-phase precursor ion-dipole complex and the gas-phase SP (Table 1). The other remaining coordinates are optimized by direct gas-phase calculations. The results are shown in Fig. 9. The diagonal elements V_{11} and V_{22} are strongly stabilized by the external electrostatic potential because the system has negative charge, and all the values of the electrostatic potential are positive. When $\mathbf{\Phi} = \mathbf{\Phi}^{\text{IDC}}$ (Fig. 9b), V_{11} is more stabilized than V_{22} because $\mathbf{\Phi}^{\text{IDC}}$ is favorable to V_{11}. Although the effect of the electrostatic potential on V_{12} is smaller than the effects on V_{11} and V_{22}, the profile of V_{12} with $\mathbf{\Phi} = \mathbf{\Phi}^{\text{IDC}}$ is asymmetric. Therefore, it is important to consider the dependence of V_{12} on external electrostatic potential $\mathbf{\Phi}$.

The charge distribution of the QM subsystem is important in QM/MM calculations since it controls the interaction with the MM subsystem. The partial charge on each atom in the EE-MCMM-9 and direct calculations along the MFEP obtained by the RISM-SCF method is presented in Fig. 10. Although there is a slight difference at $|z| > 1.5$ Å, the results of the two calculations are quite similar. Note that no Shepard points were placed at $|z| > 1.378$ Å because the ion-dipole complexes are located at $|z| = 1.378$ Å in the gas phase. If Shepard points are added in such regions, the results will be improved.

5. Conclusion

In the present work, we proposed a method for generating a potential energy function for a system in the presence of an electrostatic potential. For this purpose, we extended the MCMM method so that the potential energy depends on the electrostatic potential acting on the atomic centers of a subsystem, which is called the QM subsystem. The resulting energy representation can be used to describe PESs defined by a QM/MM method. The charge distribution of the QM subsystem can be obtained by calculating the derivative of the potential energy with respect to the electrostatic potential distribution.

We applied the present method to the degenerate rearrangement $Cl^- + CH_3Cl' \rightarrow ClCH_3 + Cl'^-$ in aqueous solution. We first generated the semi-global PES in the gas phase by the original MCMM method, and then we generated it in aqueous solution using the same electronic structure information augmented by a Maclaurin series with respect to the electrostatic potential distribution. The calculated potential energy in aqueous solution is very close to that calculated directly without any fitting. The charge distribution in aqueous solution as calculated by the present method is also found to be quite similar to that obtained directly. This shows that we can generate a semi-global PES in the condensed phase using only electronic structure information in gas phase. From the perspective of computational cost, it is very efficient that we can use only gas-phase data to determine the location of the Shepard points (in both coordinate space and electrostatic potential distribution space) when we apply the present method to reactions in the condensed phase.

Based on the present results, we conclude that the new EE-MCMM method is a very powerful tool for studying reactions in the condensed phase. Although we didn't present the results of actual MD simulations here, such applications are now straightforward. An application of the present method to the MD simulation of a condensed-phase reaction is now in progress.

References

(1)   Warshel, A.; Levitt, M. *J. Mol. Biol.* **1976**, *103*, 227.

(2)   Field, M. J.; Bash, P. A. ; Karplus, M. *J. Comput. Chem.* **1990**, *11*, 700.

(3)   Gao, J. *Acc. Chem. Res.* **1996**, *29*, 298.

(4)   Bakowies, D.; Thiel, W. *J. Phys. Chem.* **1996**, *100*, 10580.

(5)   Eurenius, K. P.; Chatfield, D. C.; Brooks, B. R.; Hodoscek, M. *Int. J. Quantum Chem.* **1996**, *60*, 1189.

(6)   Truong, T. N.; Truong, T.-T.; Stefanovich, E. V. *J. Chem. Phys.* **1997**, *107*, 1881.

(7)   Tongraar, A.; Liedl, K. R.; Rode, B. M. *J. Phys. Chem. A* **1998**, *102*, 10340.

(8)   Zhang, Y.; Lee, T.-S.; Yang, W. *J. Chem. Phys.* **1999**, *110*, 46.

(9)   Philipp, D. M.; Friesner, R. A. *J. Comput. Chem.* **1999**, *20*, 1468.

(10)   Eichinger, M.; Tavan, P.; Hutter, J.; Parrinello, M. *J. Chem. Phys.* **1999**, *110*, 10452.

(11)   Woo, T. K.; Blöchl, P. E.; Ziegler, T. *J. Phys. Chem. A* **2000**, *104*, 121.

(12)   Reuter, N.; Dejaegere, A.; Maigret, B.; Karplus, M. *J. Phys. Chem. A* **2000**, *104*, 1720.

(13)   Gogonea, V.; Westerhoff, L. M.; Merz, K. M. Jr. *J. Chem. Phys.* **2000**, *113*, 5604.

(14)   Chalmet, S.; Rinaldi, D.; Ruiz-Lopez, M. F. *Int. J. Quantum Chem.* **2001**, *84*, 559.

(15)   Martí, S.; Andrés, J.; Moliner, V.; Silla, E.; Tuñón, I.; Bertrán, J. *Theor. Chem. Acc.* **2001**, *105*, 207.

(16)   Gao, J.; Truhlar, D. G. *Annu. Rev. Phys. Chem.* **2002**, *53*, 467.

(17)   Laio, A.; VandeVondele, J.; Rothlisberger, U. *J. Chem. Phys.* **2002**, *116*, 6941.

(18)   Amara, P.; Field, M. J. *Theor. Chem. Acc.* **2003**, *109*, 43.

(19)   Vreven, T.; Morokuma, K. *Theor. Chem. Acc.* **2003**, *109*, 125.

(20)   Kerdcharoen, T.; Birkenheuer, U.; Krüger, S.; Woiterski, A.; Rösch, N. *Theor. Chem. Acc.* **2003**, *109*, 285.

(21)   Nemukhin, A. V.; Grigorenko, B. L.; Topol, I. A.; Burt, S. K. *J. Comput. Chem.* **2003**, *24*, 1410.

(22)   Toniolo, A.; Ciminelli, C.; Granucci, G.; Laino, T.; Persico, M. *Theor. Chem. Acc.* **2004**, *111*, 270.

(23)   Bathelt, C. M.; Zurek, J.; Mulholland, A. J.; Harvey, J. N. *J. Am. Chem. Soc.* **2005**, *127*, 12900.

(24)   Sundararajan, M.; Hillier, I. H.; Burton, N. A. *J. Phys. Chem. A* **2006**, *110*, 785.

(25)   Riccardi, D.; Schaefer, P.; Yang, Y.; Yu, H.; Ghosh, N.; Prat-Resina, X.; König, P.; Li, G.; Xu, D.; Guo, H.; Elstner, M.; Cui, Q. *J. Phys. Chem. B* **2006**, *110*, 6458.

(26)   To, J.; Sherwood, P.; Sokol, A. A.; Bush, I. J.; Catlow, C. R. A.; van Dam, H. J. J.; French, S. A.; Guest, M. F. *J. Mat. Chem.* **2006**, *16*, 1919.

(27)   Lin, H.; Truhlar, D. G. *Theor. Chem. Acc.* **2007**, *117*, 185.

(28)   Senn, H. M.; Thiel, W. *Curr. Opinion Chem. Biol.* **2007**, *11*, 182.

(29)   Chandrasekhar, J.; Smith, S. F.; Jorgensen, W. L. *J. Am. Chem. Soc.* **1985**, *107*, 154.

(30)   Zhang, Y.; Liu, H.; Yang, W. *J. Chem. Phys.* **2000**, *112*, 3483.

(31)   Kollman, P. A.; Kuhn, B.; Donini, O.; Perakyla, M.; Stanton, R.; Bakowies, D. *Acc. Chem. Res.* **2001**, *34*, 72.

(32)   Ishida, T.; Kato, S. *J. Am. Chem. Soc.* **2003**, *125*, 12035.

(33)   Xie, L.; Liu, H.; Yang, W. *J. Chem. Phys.* **2004**, *120*, 8039.

(34)   Liu, H.; Lu, Z.; Cisneros, G. A.; Yang, W. *J. Chem. Phys.* **2004**, *121*, 697.

(35)   Cisneros, G. A.; Liu, H.; Lu, Z.; Yang, W. *J. Chem. Phys.* **2005**, *122*, 114502.

(36)   Rod, T. H.; Ryde, U. *J. Chem. Theory Comput.* **2005**, *1*, 1240.

(37)   Lu, Z.; Yang, W. *J. Chem. Phys.* **2004**, *121*, 89.

(38)   Radkiewicz, J. L.; Brooks, C. L. III *J. Am. Chem. Soc.* **2000**, *122*, 225.

(39)   Truhlar, D. G.; Gao, J.; Alhambra, C.; Garcia-Viloca, M.; Corchado, J.; Sanchez, M. L.; Villa, J. *Acc. Chem. Res.* **2002**, *35*, 341.

(40)   Truhlar, D. G.; Gao, J.; Garcia-Viloca, M.; Alhambra, C.; Corchado, J.; Sanchez, M. L.; Poulsen, T. D. *Int. J. Quantum Chem.* **2004**, *100*, 1136.

(41)   Garcia-Viloca, M.; Poulsen, T. D.; Truhlar, D. G.; Gao, J. *Protein Sci.* **2004**, *13*, 2341.

(42)   Zou, P.; Osborn, D. L. *Phys. Chem. Chem. Phys.* **2004**, *6*, 1697.

(43)   Garrett, B. C.; Truhlar, D. G. In *Theory and Applications of Computational Chemistry: The First Forty Years*; Dystra, C. E., Frenking, G., Kim, K. S., Scuseria, G. E., Eds.; Elsevier: Amsterdam, 2005; p 67.

(44)   Roca, M.; Andrés, J.; Moliner, V.; Tuñón, I.; Bertrán, J. *J. Am. Chem. Soc.* **2005**, *127*, 10648.

(45)   Thorpe, I. F.; Brooks, C. L. III *J. Am. Chem. Soc.* **2005**, *127*, 12997.

(46)   Claeyssens, F.; Ranaghan, K. E.; Manby, F. R.; Harvey, J. N.; Mulholland, A. J. *Chem. Comm.* **2005**, 5068.

(47)   Pu, J.; Gao, J.; Truhlar, D. G. *Chem. Rev.* **2006**, *106*, 3140.

(48)   Ruiz-Pernía, J.; Silla, E.; Tuñón, I. *J. Phys. Chem. B* **2006**, *110*, 20686.

(49)   Rivail, J.-L.; Rinaldi, D. *Comp. Chem.: Rev. Current Trends*, **1996**, *1*, 139.

(50)   Tomasi, J.; Persico, M. *Chem. Rev.* **1994**, *94*, 2027.

(51)   Tomasi, J.; Mennucci, B.; Cammi, R. *Chem. Rev.* **2005**, *105*, 2999.

(52)   Cramer, C. J.; Truhlar, D. G. *J. Am. Chem. Soc.* **1991**, *113*, 8305.

(53)   Cramer, C. J.; Truhlar, D. G. *Chem. Rev.* **1999**, *99*, 2161.

(54)   Bashford, D.; Case, D. A. *Annu. Rev. Phys. Chem.* **2000**, *51*, 129.

(55)   Ten-no, S.; Hirata, F.; Kato, S. *Chem. Phys. Lett.* **1993**, *214*, 391.

(56)   Ten-no, S.; Hirata, F.; Kato, S. *J. Chem. Phys.* **1994**, *100*, 7443.

(57)   Sato, H.; Hirata, F.; Kato, S. *J. Chem. Phys.* **1996**, *105*, 1546.

(58)   Sato, H. *Understanding Chem. React.* **2003**, *24*, 61.

(59)   Chuang, Y.-Y.; Cramer, C. J.; Truhlar, D. G. *Int. J. Quantum Chem.* **1998**, *70*, 887.

(60)   Chuang, Y.-Y.; Radhakrishnan, M. L.; Fast, P. L.; Cramer, C. J.; Truhlar, D. G. *J. Phys. Chem. A* **1999**, *103*, 4893.

(61)   Hu, H.; Lu, Z.; Yang, W. *J. Chem. Theory Comput.* **2007**, *3*, 390.

(62)   Truhlar, D. G.; Liu, Y.-P.; Schenter, G. K.; Garrett, B. C. *J. Phys. Chem.* **1994**, *98*, 8396.

(63)   Galván, I. F.; Martín, M. E.; Aguilar, M. A. *J Comput. Chem.* **2004**, *25*, 1227.

(64)   Dewar, M. J. S.; Zoebich, E. G.; Healy, E. F.; Stewart, J. J. P. *J. Am. Chem. Soc.* **1985**, *107*, 3902.

(65)   Stewart, J. J. P. *J. Comput. Chem.* **1989**, *10*, 209.

(66)   Elstner, M.; Porezag, D.; Jungnickel, G.; Elsner, J.; Haugk, M.; Frauenheim, T.; Suhai, S.; Seifert, G. *Phys. Rev. B* **1998**, *58*, 7260.

(67)   Frauenheim, T.; Seifert, G.; Elstner, M.; Hajnal, Z.; Jungnickel, G.; Porezag, D.; Suhai, S.; Scholz, R. *Phys. Status Solidi B* **2000**, *217*, 41.

(68)   Hofacker, G. L. *Z. Naturforoch. A* **1963**, *18*, 607.

(69)   Fukui, K.; Kato, S.; Fujimoto, H. *J. Am. Chem. Soc.* **1975**, *97*, 1.

(70)   Garrett, B. C.; Truhlar, D. G. *J. Am. Chem. Soc.* **1979**, *101*, 4534.

(71)   Morokuma, K.; Kato, S. In *Potential Energy Surfaces and Dynamics Calculations*; Truhlar, D. G., Ed.; Plenum: New York, 1981, pp. 243-264.

(72)   Miller, W. H. In *Potential Energy Surfaces and Dynamics Calculations*; Truhlar, D. G., Ed.; Plenum: New York, 1981, pp. 265-286.

(73)   Truhlar, D. G.; Brown, F. B.; Steckler, R.; Isaacson, A. D. In *The Theory of Chemical Reaction Dynamics*; Clary, D. C., Ed.; NATO ASI Series C, 70; Reidel: Dordrecht, 1986, pp. 285-329.

(74)   Fernandez-Ramos, A.; Ellingson, B. A.; Garrett, B. C.; Truhlar, D. G. *Rev. Comp. Chem. Chem.* **2007**, *23*, 125.

(75)   Kim, Y.; Corchado, J. C.; Villa, J.; Xing, J.; Truhlar, D. G. *J. Chem. Phys.* **2000**, *112*, 2718.

(76)   Albu, T. V.; Corchado, J. C.; Truhlar, D. G. *J. Phys. Chem. A* **2001**, *105*, 8465.

(77)   Lin, H.; Pu, J.; Albu, T. V.; Truhlar, D. G. *J. Phys. Chem. A* **2004**, *108*, 4112.

(78)   Kim, K. H.; Kim, Y. *J. Chem. Phys.* **2004**, *120*, 623.

(79)   Kim, Y.; Kim, Y. *J. Phys. Chem. A* **2006**, *110*, 600.

(80)   Lin, H.; Zhao, Y.; Tishchenko, O.; Truhlar, D. G. *J. Chem. Theory Comput.* **2006**, *2*, 1237.

(81)   Tishchenko, O.; Truhlar, D. G. *J. Phys. Chem. A* **2006**, *110*, 13530.

(82)   Tishchenko, O.; Truhlar, D. G. *J. Chem. Theory Comput.* **2007**, *3*, 938.

(83)   Truhlar, D. G. *J. Phys. Chem. A* **2002**, *106*, 5048.

(84)   Albu, T. V.; Espinosa-García, J.; Truhlar, D. G. *Chem. Rev.* **2007**, *107*, 5101.

(85)   Ischtwan, J.; Collins, M. A. *J. Chem. Phys.* **1994**, *100*, 8080.

(86)   Nguyen, K. A.; Rossi, I.; Truhlar, D. G. *J. Chem. Phys.* **1995**, *103*, 5522.

(87)   Chandrasekhar, J.; Smith, S. F.; Jorgensen, W. L. *J. Am. Chem. Soc.* **1984**, *106*, 3049.

(88)   Bash, P. A.; Field, M. J.; Karplus, M. *J. Am. Chem. Soc.* **1987**, *109*, 8092.

(89)   Kozaki, T.; Morihashi, K.; Kikuchi, O. *J. Am. Chem. Soc.* **1989**, *111*, 1547.

(90)   Huston, S. E.; Rossky, P. J.; Zichi, D. A. *J. Am. Chem. Soc.* **1989**, *111*, 5680.

(91)   Tucker, S. C.; Truhlar, D. G. *J. Am. Chem. Soc.* **1990**, *112*, 3347-3361.

(92)   Zhao, X. G.; Tucker, S. C.; Truhlar, D. G. *J. Am. Chem. Soc.* **1991**, *113*, 826.

(93)   Basilevsky, M. V.; Chudinov, G. E.; Napolov, D. V. *J. Phys. Chem.* **1993**, *97*, 3270.

(94)   Mathis, J. R.; Bianco, R.; Hynes, J. T. *J.Mol. Liq.* **1994**, *61*, 81.

(95)   Truong, T. N.; Stefanovich, E. V. *J. Phys. Chem.* **1995**, *99*, 14700.

(96)   Pomelli, C. S.; Tomasi, J. *J. Phys. Chem. A* **1997**, *101*, 3561.

(97)   Cossi, M.; Adamo, C.; Barone, V. *Chem. Phys. Lett.* **1998**, *297*, 1.

(98)   Mo, Y.; Gao, J. *J. Comput. Chem.* **2000**, *21*, 1458.

(99)   Safi, B.; Choho, K.; Geerlings, P. *J. Phys. Chem. A* **2001**, *105*, 591.

(100)   Ohmiya, K.; Kato, S. *Chem. Phys. Lett.* **2001**, *348*, 75.

(101)   Gao, J.; Garcia-Viloca, M.; Poulsen, T. D.; Mo, Y. *Adv. Phys. Org. Chem.* **2003**, *38*, 161.

(102)   Mo, S. J.; Vreven, T.; Mennucci, B.; Morokuma, K.; Tomasi, J. *Theor. Chem. Acc.* **2004**, *111*, 154.

(103)   Vayner, G.; Houk, K. N.; Jorgensen, W. L.; Brauman, J. I. *J. Am. Chem. Soc.* **2004**, *126*, 9054.

(104)   Sato, H.; Sakaki, S. *J. Phys. Chem. A* **2004**, *108*, 1629.

(105)   Freedman, H.; Truong, T. N. *J. Phys. Chem. B* **2005**, *109*, 4726.

(106)   Song, L.; Wu, W.; Hiberty, P. C.; Shaik, S. *Chem. Eur. J.* **2006**, *12*, 7458.

(107)   Casanova, D.; Gusarov, S.; Kovalenko, A.; Ziegler, T. *J. Chem. Theory Comput.* **2007**, *3*, 458.

(108) Su, P.; Wu, W.; Kelly, C. P.; Cramer, C. J.; Truhlar, D. G. *J. Phys. Chem. A*, to be published.

(109) Bayly, C. I.; Cieplak, P.; Cornell, W. D.; Kollman, P. A. *J. Phys. Chem.* **1993**, *97*, 10269.

(110) Morita, A.; Kato, S. *J. Am. Chem. Soc.* **1997**, *119*, 4021.

(111) Morita, A.; Kato, S. *J. Chem. Phys.* **1998**, *108*, 6809.

(112) Hayashi, S.; Ohmine, I. *J. Phys. Chem. B* **2000**, *104*, 10678.

(113) Wilson, E. B. Jr.; Decius, J. C.; Cross, P. C. *Molecular Vibrations*; Dover: New York, 1955.

(114) Chang, Y.-T.; Miller, W. H. *J. Phys. Chem.* **1990**, *94*, 5884.

(115) Lynch, B. J.; Fast, P. L.; Harris, M.; Truhlar, D. G. *J. Phys. Chem. A* **2000**, *104*, 4811.

(116) Kelly, C. P.; Cramer, C. J.; Truhlar, D. G. *J. Chem. Theory Comput.* **2005**, *1*, 1133.

(117) Mayer, I. *Chem. Phys. Lett.* **1983**, *97*, 270.

(118) Mayer, I. *Chem. Phys. Lett.* **1985**, *117*, 396.

(119) Mayer, I. *Int. J. Quantum Chem.* **1986**, *29*, 477.

(120) Thompson, J. D.; Xidos, J. D.; Sonbuchner, T. M.; Cramer, C. J.; Truhlar, D. G. *PhysChemComm* **2002**, 117.

(121) Zhu, T.; Li, J.; Hawkins, G. D.; Cramer, C. J.; Truhlar, D. G. *J. Chem. Phys.* **1998**, *109*, 9117.

(122) Zhu, T.; Li, J.; Liotard, D. A.; Cramer, C. J.; Truhlar, D. G. *J. Chem. Phys.* **1999**, *110*, 5503.

(123)   Albu, T. V.; Tishchenko, O.; Corchado, J. C.; Kim, Y.; Villà, J.; Xing, J.; Lin, H.; Truhlar, D. G.; MC-TINKERATE–version 2007; University of Minnesota: Minneapolis, MN, 2007.

(124)   Isaacson, A. D.; Truhlar, D. G. *J. Chem. Phys.* **1982**, *76*, 1380.

(125)   Kirkwood, J. G. *J. Chem. Phys.* **1935**, *3*, 300.

(126)   Hill, T. L. *Statistical Mechanics: Principles and Selected Applications*; Dover: New York, 1956; pp. 193-194.

(127)   Kinoshita, M. *Understanding Chem. React.* **2003**, *14*, 101.

(128)   Hirata, F. *Understanding Chem. React.* **2003**, *24*, 1.

(129)   Singer, S. J.; Chandler, D. *Mol. Phys.* **1985**, *55*, 621.

(130)   Cornell, W. D.; Cieplak, P.; Bayly, C. I.; Gould, I. R.; Merz Jr, K. M.; Ferguson, D. M.; Spellmeyer, D. G.; Fox, T.; Caldwell, J. W.; Kollman, P. A. *J. Am. Chem. Soc.* **1995**, *117*, 5179.

(131)   Berendsen, H. J. C.; Postma, J. P. M.; van Gunsteren, W. P.; Hermans, J.; B. Pullman (eds.) *Intermolecular Forces*; Reidel, Dordrecht, 1981.

(132)   Chamberlin, A. C.; Pu, J.; Kelly, C. P.; Thompson, J. D.; Xidos, J. D.; Li, J.; Zhu, T.; Hawkins, G. D.; Chuang, Y.-Y.; Fast, P. L.; Lynch, B. J.; Liotard, D. A.; Rinaldi, D.; Gao, J.; Cramer, C. J.; Truhlar, D. G.; GAMESSPLUS–version 4.8.; University of Minnesota: Minneapolis, 2006.

(133)   Schmidt, M. W.; Baldridge, K. K.; Boatz, J. A.; Elbert, S. T.; Gordon, M. S.; Jensen, J. H.; Koseki, S.; Matsunaga, N.; Nguyen, K. A.; Su, S. J.; Windus, T. L.; Dupuis, M.; Montgomery, J. A. *J. Comput. Chem.* **1993**, *14*, 1347.

(134)   Allinger, N. L.; Yuh, Y. H.; Lii, J. H. *J. Am. Chem. Soc.* **1989**, *111*, 8551.

(135) Lii, J. H.; Allinger, N. L. *J. Am. Chem. Soc.* **1989**, *111*, 8566.

(136) Lii, J. H.; Allinger, N. L. *J. Am. Chem. Soc.* **1989**, *111*, 8576.

(137) Herzberg, G. *Molecular Spectra and Molecular Structure. I. Spectra of Diatomic Molecules*; 2nd ed.; D. Van Nostrand: Princeton, 1950;p. 101.

(138) Linstrom, P. J.; Mallard, W. G., (Eds.); NIST Chemistry WebBook, NIST Standard Reference Database Number 69, National Institute of Standards and Technology: Gaithersburg, MD, 2005, http://webbook.nist.gov.

(139) Ponder, J. W.; TINKER–version 3.5; Washington University: St. Louis, MO, 1997.

(140) Tishchenko, O.; Albu, T. V.; Corchado, J. C.; Kim, Y.; Villà, J.; Xing, J.; Lin, H.; Truhlar, D. G.; MC-TINKER–version 2007; University of Minnesota: Minneapolis, MN, 2007.

(141) Li, C.; Ross, P.; Szulejko, J. E.; McMahon, T. B. *J. Am. Chem. Soc.* **1996**, *118*, 9360.

(142) Wladkowski, B. D.; Brauman, J. I. *J. Phys. Chem.* **1993**, *97*, 13158.

(143) Zhao, Y.; Gonzalez-Garcia, N.; Truhlar, D. G. *J. Phys. Chem. A* **2005**, *109*, 2012.

(144) McLennan, D. J. *Aust. J. Chem.* **1978**, *31*, 1897.

Table 1. Electrostatic potential (in volts) on each atom in aqueous solution by RISM-SCF at the gas-phase ion-dipole complex and the gas-phase saddle point.

	Ion-dipole complex	Saddle point
Φ_C	4.467	4.753
Φ_H	4.596	4.611
$\Phi_{Cl'}$	3.552	5.211
Φ_{Cl}	7.048	5.211

Table 2. Partial charges (in units of e) and electrostatically embedded QM energy (in kcal/mol) in the gas phase and in aqueous solution.

	Gas phase	Solution phase		
	direct	direct	EE-MCMM	Original CRK
		Ion-dipole complex [a]		
Q_C	-0.1447	-0.1570	-0.1558	-0.1480
Q_H	0.1157	0.1117	0.1109	0.1110
$Q_{Cl'}$	-0.2559	-0.2036	-0.2072	-0.2093
Q_{Cl}	-0.9425	-0.9744	-0.9699	-0.9751
V^{EEQM}	-9.67	-163.82	-163.72	-163.76
		Saddle point [a]		
Q_C	-0.0260	-0.0157	-0.0153	-0.0155
Q_H	0.1185	0.1265	0.1264	0.1263
$Q_{Cl}\left(=Q_{Cl'}\right)$	-0.6448	-0.6820	-0.6819	-0.6817
V^{EEQM}	3.19	-121.86	-121.85	-121.85

[a] Gas-phase geometries.

Figure 1. Energy profiles of the $Cl^- + CH_3Cl \rightarrow ClCH_3 + Cl^-$ reaction: PES profile for gas-phase reaction along the direct MEP (solid) and FES profile for the reaction in aqueous solution along the direct MFEP calculated by RISM-SCF (dashed). Both curves are relative to reactants ($z = -\infty$).

Figure 2. Gas-phase calculations: two-dimensional representation of the direct MEP and the location of Shepard points for the MCMM-9 calculation. Filled circles are stationary points, and open circles are other Shepard points.

Figure 3. Gas-phase potential energy profiles along the MEP as a function of the reaction coordinate z: direct (solid line), MCMM-0 (dashed line), MCMM-4 (dotted line) and MCMM-8 (dot-dashed line). The dot-dashed line is almost completely hidden by the solid one. All curves are plotted for the direct MEP.

Figure 4. (a) Equipotential contours of the gas-phase PES calculated by MCMM-9. Contour labels are in kcal/mol. Countours are spaced from -8 to 8 by 2 kcal/mol. The zero of energy is at infinitely separated reagents. (b) Equipotential contours of the difference between the gas-phase PESs calculated by the MCMM-9 and direct methods. Contours are spaced from -5 to 5 by 2 kcal/mol.

Figure 5. The matrix elements of the electronically diabatic Hamiltonian $\mathbf{V}^{\text{MCMM}}$ and the lowest eigenvalue V^{MCMM} along the paths with (a) $R_{\text{CCl}} + R_{\text{CCl}'} = 4.6$ Å, (b) $R_{\text{CCl}} + R_{\text{CCl}'} = 5.0$ Å, (c) $R_{\text{CCl}} = 1.8$ Å, and (d) $R_{\text{CCl}} = 2.3$ Å.

Figure 6. Partial charge on each atom in the EE-MCMM-9 (left) and direct (right) calculations: partial charge on C (solid line), H (dashed line), Cl′ (dotted line) and Cl (dot-dashed line).

Figure 7. Potential energy profiles along the direct aqueous-phase MFEP: direct RISM-SCF (solid line); EE-MCMM-9 (dashed line).

Figure 8. (a) Equipotential contours of the PES calculated by the EE-MCMM-9. Contour labels are in kcal/mol. Countours are spaced from -170 to -110 by 10 kcal/mol. (b) equipotential contours of the difference between the PESs calculated by the EE-MCMM-9 and direct methods. Countours are spaced from -5 to 5 by 2 kcal/mol.

Figure 9. The matrix elements of the electronically diabatic Hamiltonian $\mathbf{V}^{\text{EE-MCMM}}$ and the lowest eigenvalue $V^{\text{EE-MCMM}}$ along the path with $R_{\text{CCl}} + R_{\text{CCl'}} = 4.8$ Å for the electrostatic potential distributions with (a) $\mathbf{\Phi} = \mathbf{0}$, (b) $\mathbf{\Phi} = \mathbf{\Phi}^{\text{IDC}}$, (c) $\mathbf{\Phi} = \mathbf{\Phi}^{\text{SP}}$, and (d) $\mathbf{\Phi} = \frac{1}{2}\mathbf{\Phi}^{\text{SP}}$.

Figure 10. Partial charge on each atom in the EE-MCMM-9 (left) and direct calculations (right) along the MFEP obtained by RISM-SCF method: partial charge on C (solid line), H (dashed line), Cl′ (dotted line) and Cl (dot-dashed line).
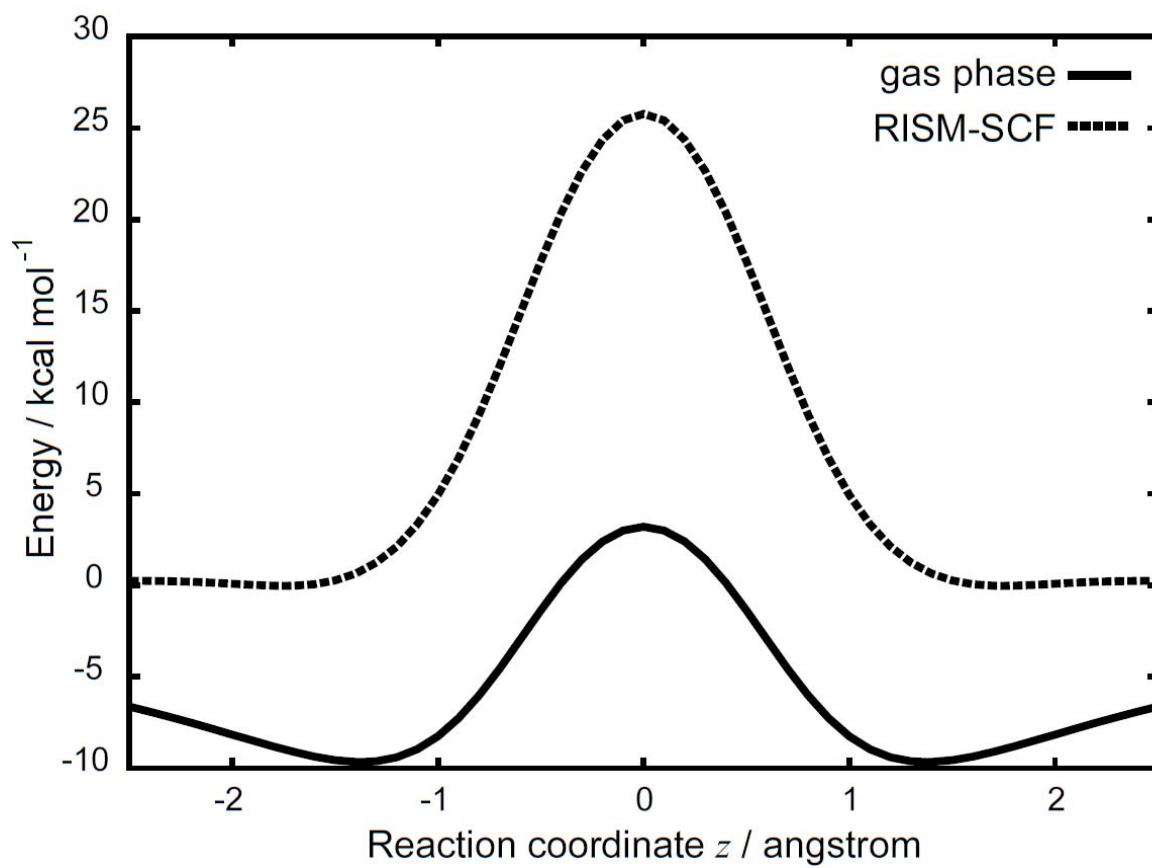
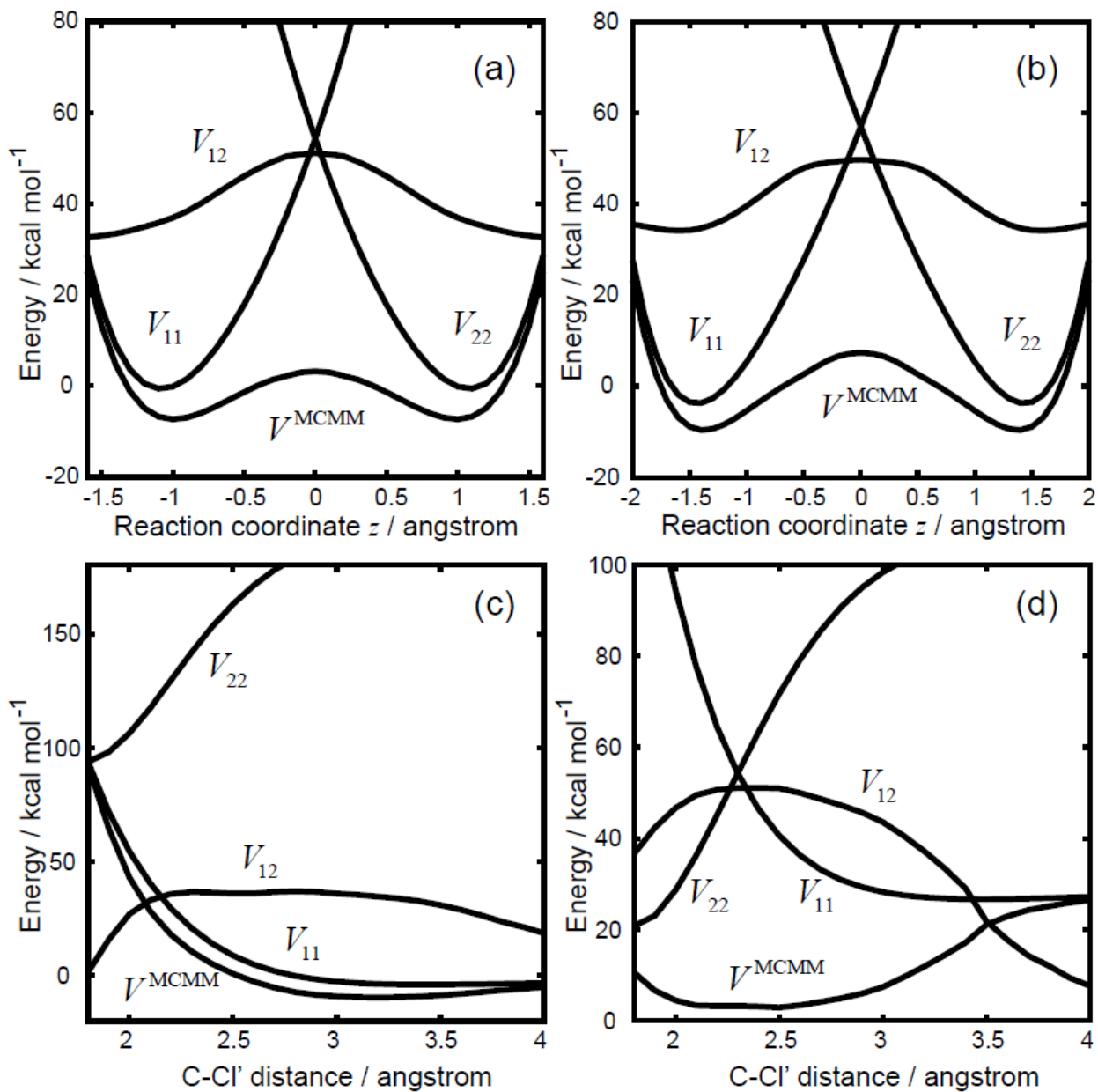M. Higashi and D. G. Truhlar, Figure 1.
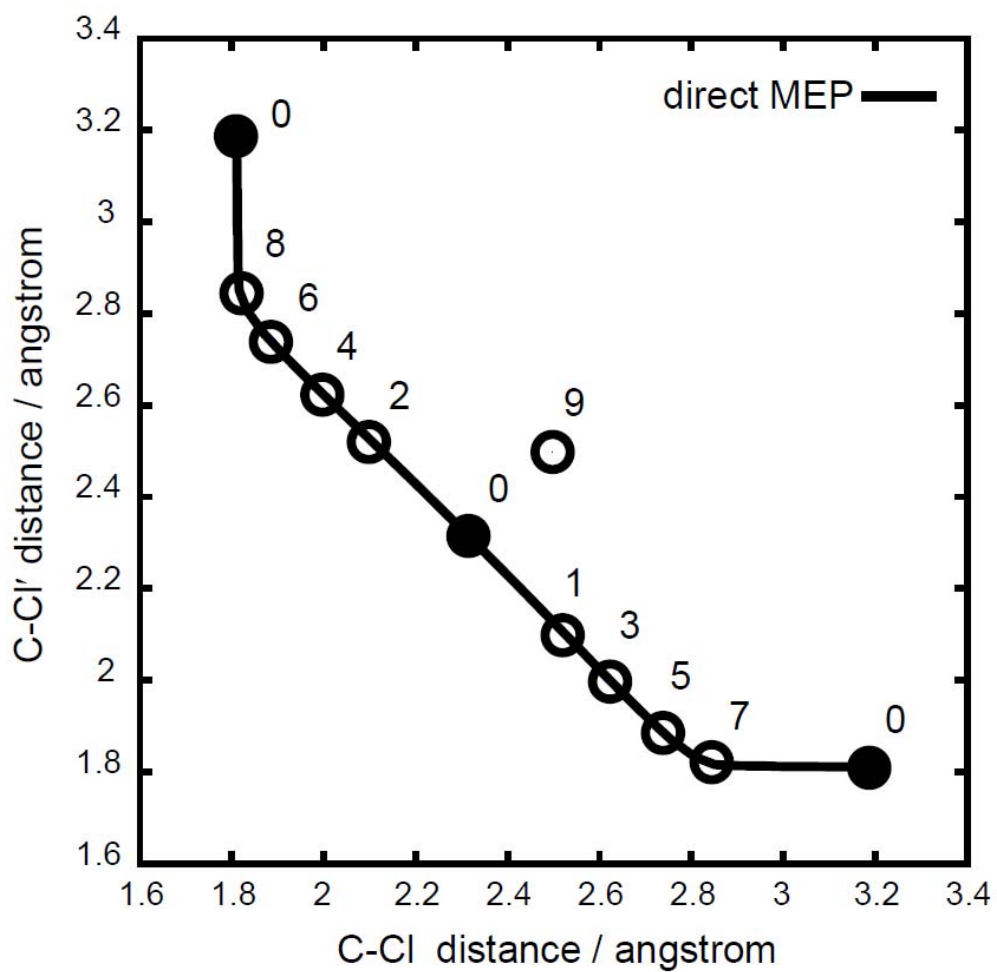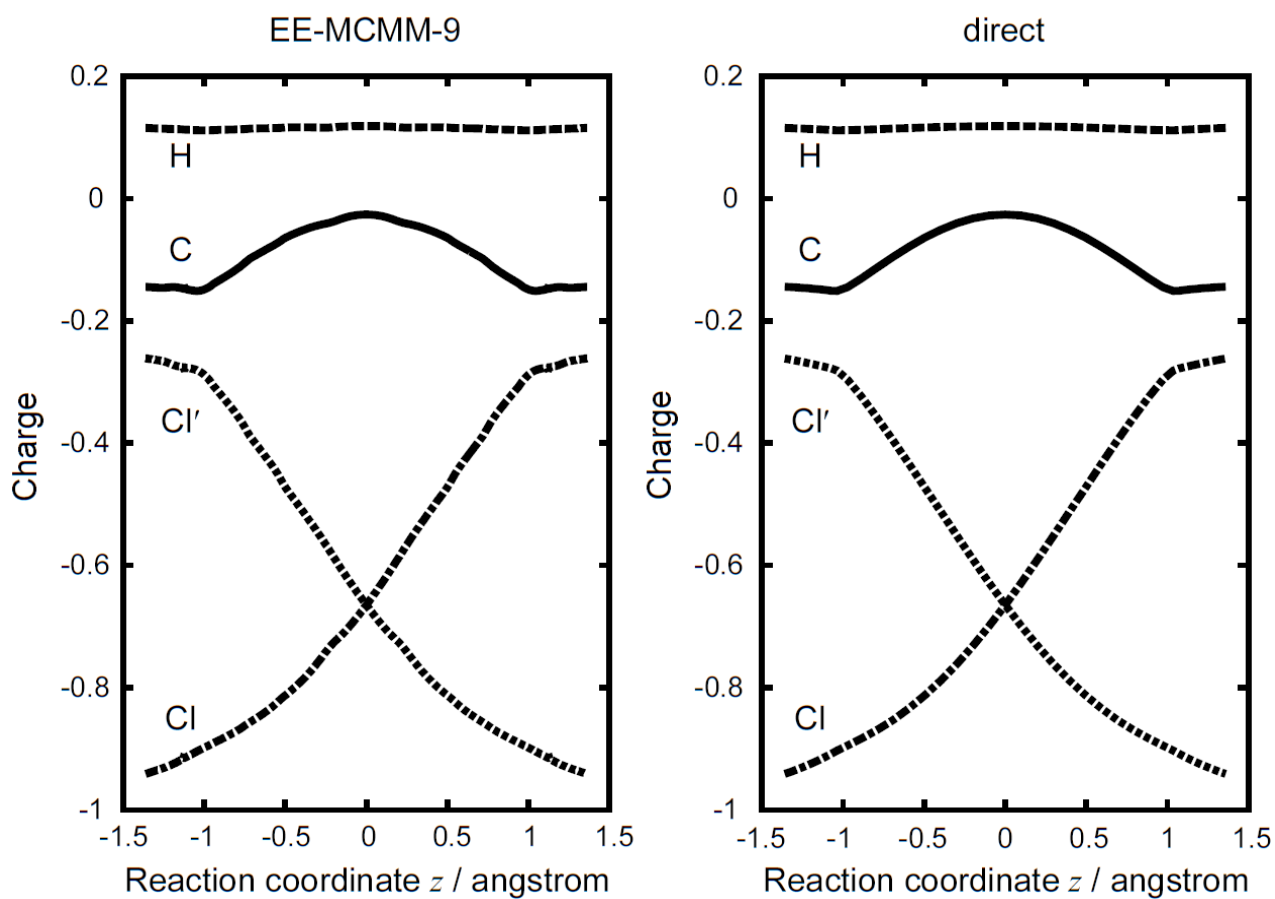
M. Higashi and D. G. Truhlar, Figure 2.
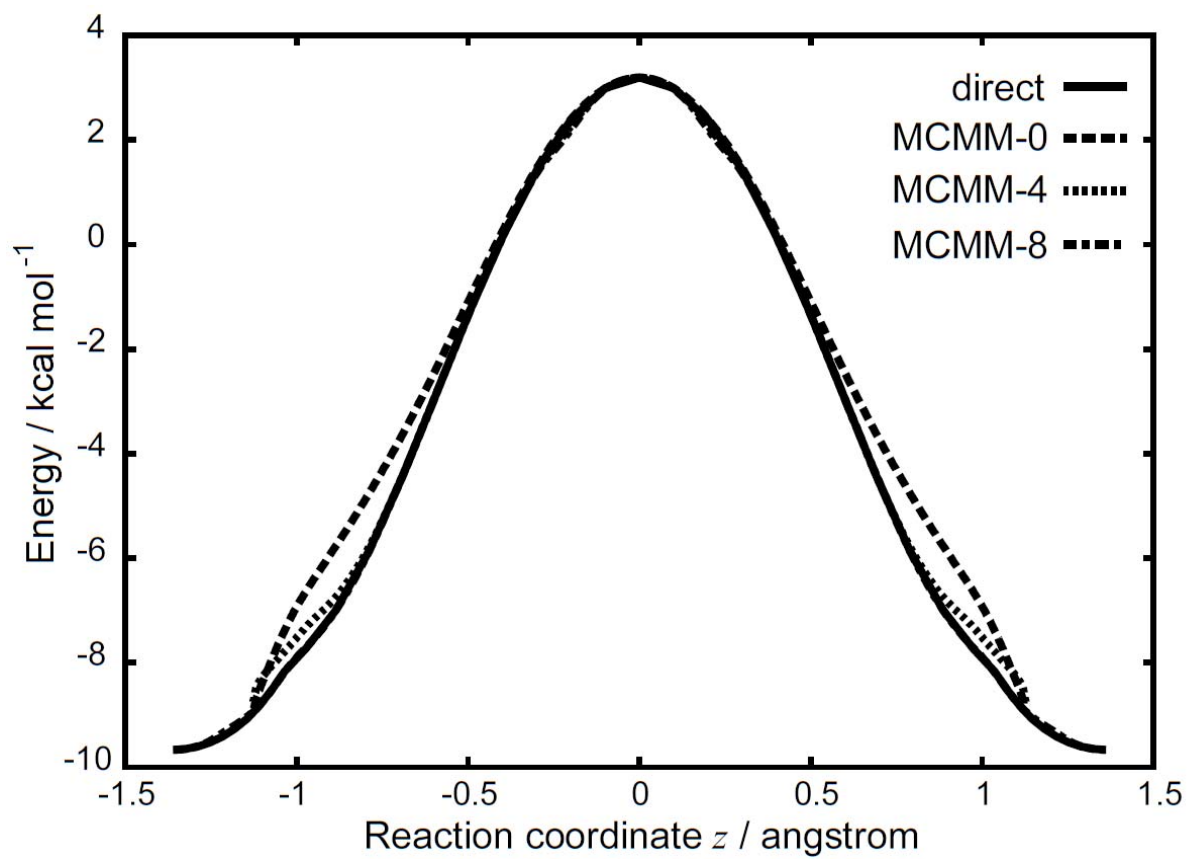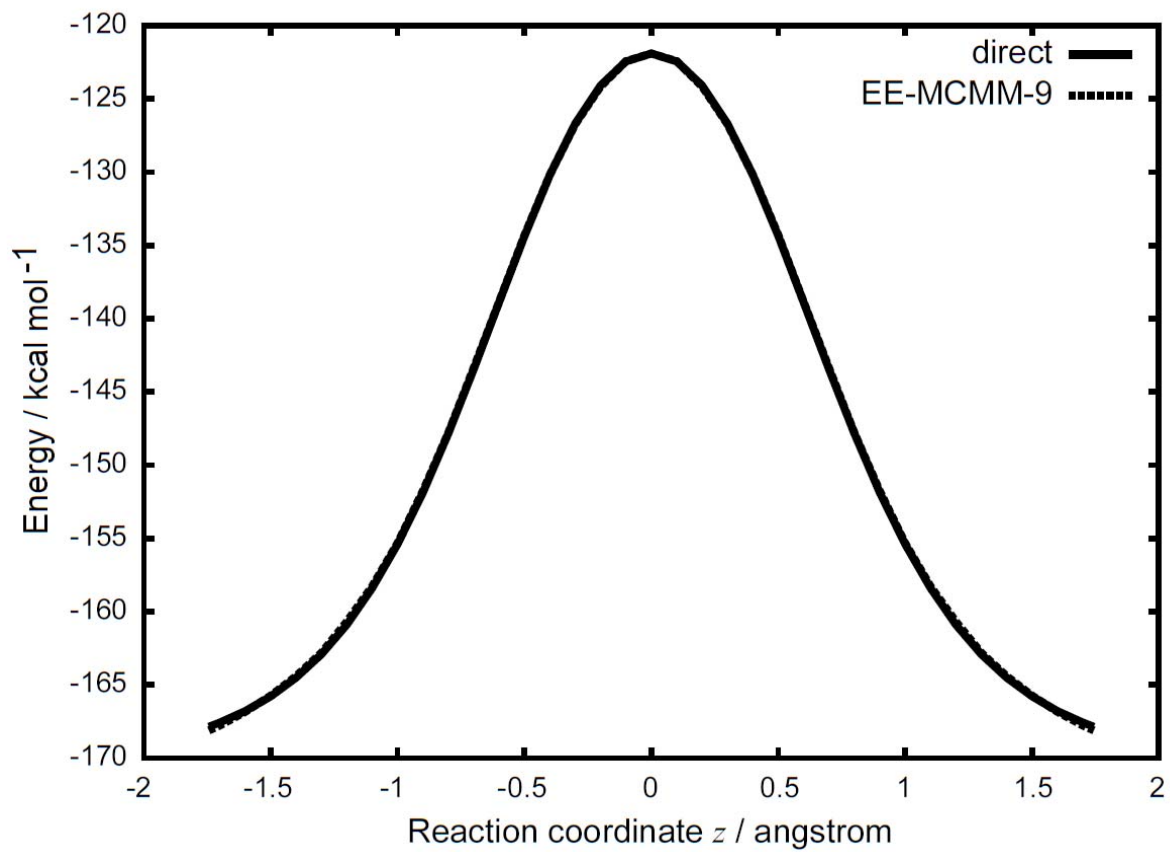
M. Higashi and D. G. Truhlar, Figure 3.
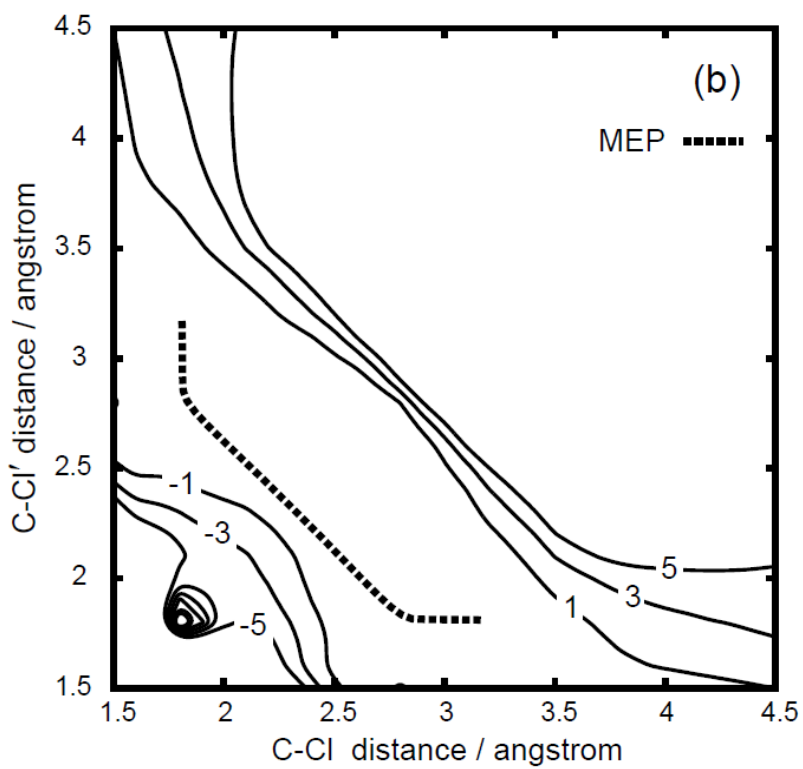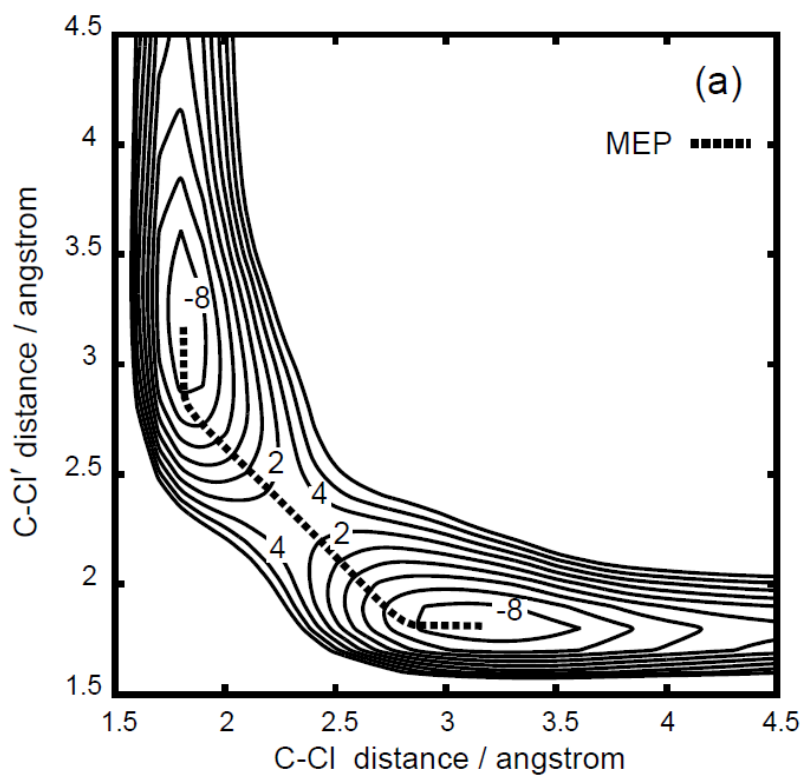
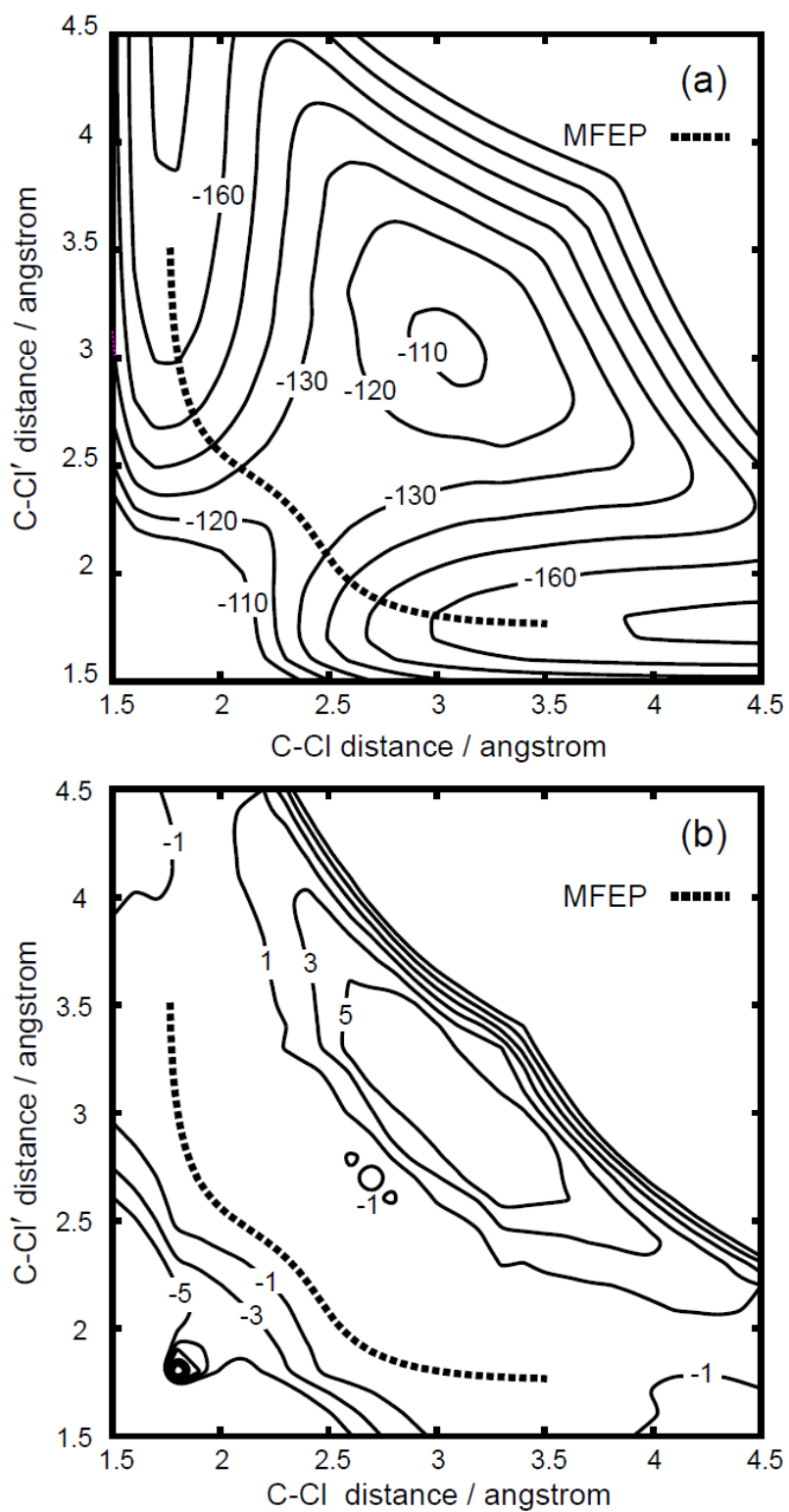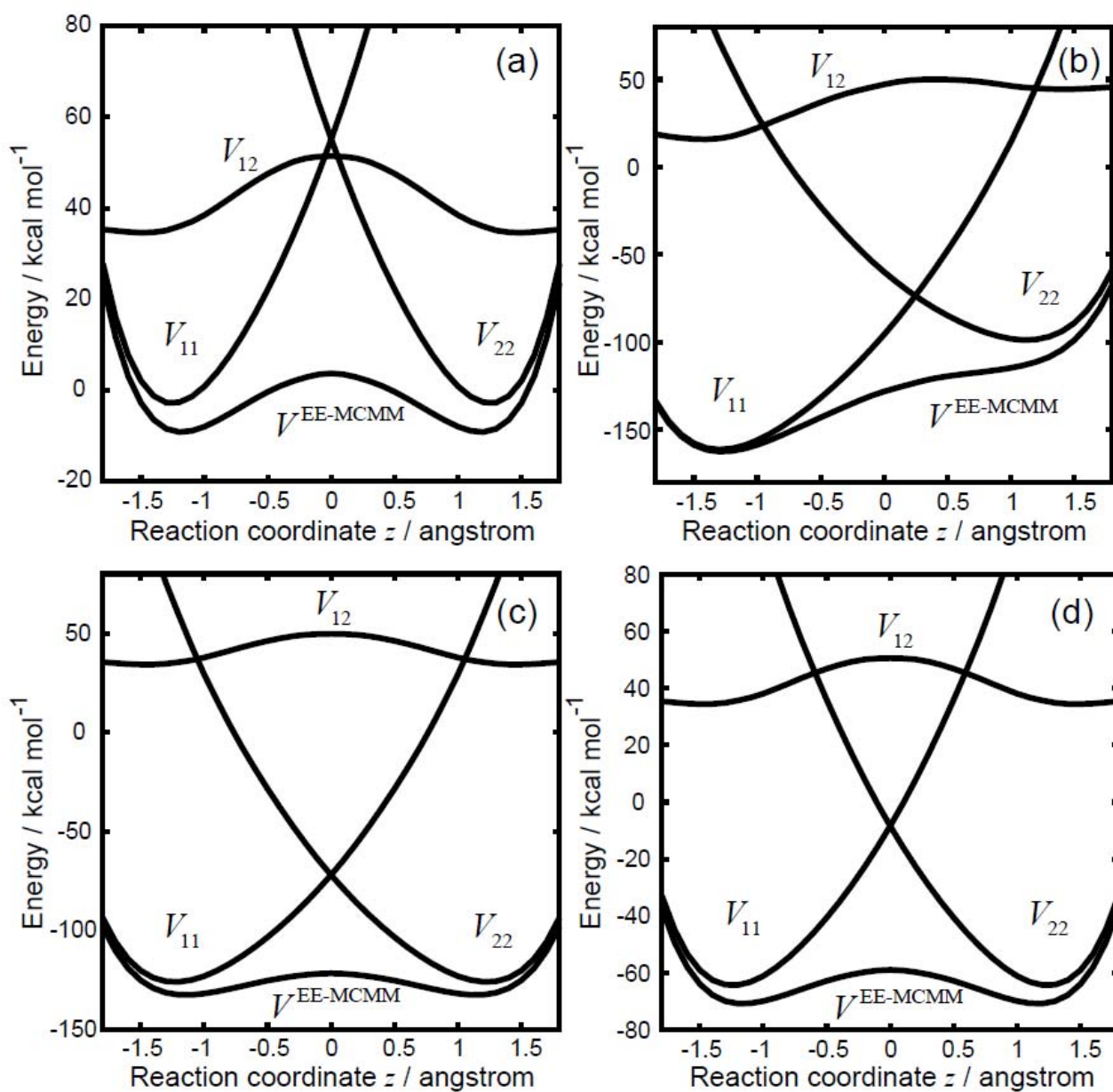M. Higashi and D. G. Truhlar, Figure 4.

M. Higashi and D. G. Truhlar, Figure 5.

M. Higashi and D. G. Truhlar, Figure 6.

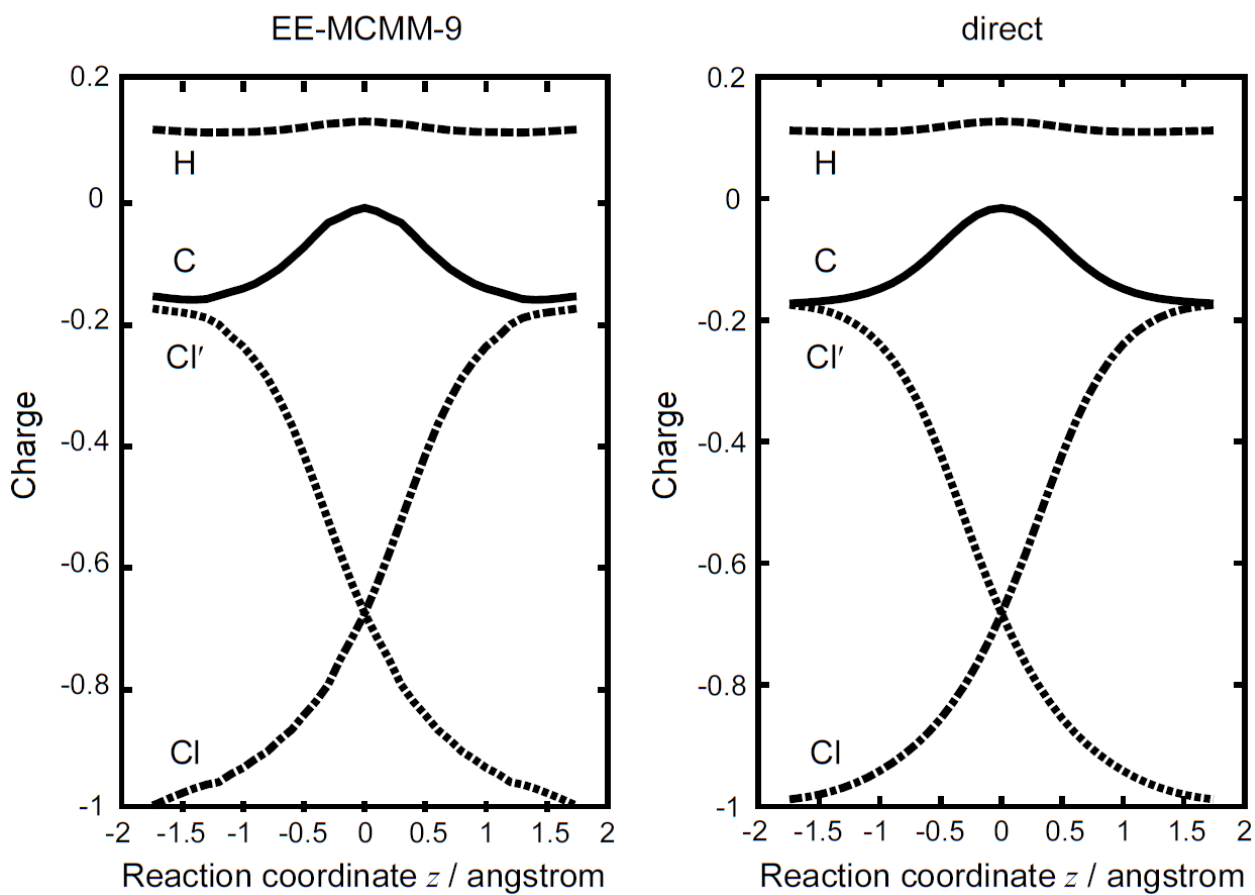M. Higashi and D. G. Truhlar, Figure 7.

M. Higashi and D. G. Truhlar, Figure 8.

M. Higashi and D. G. Truhlar, Figure 9.

M. Higashi and D. G. Truhlar, Figure 10.